Solid Earth, 17, 407–427, 2026
https://doi.org/10.5194/se-17-407-2026

Solid Earth Open Access EGU

Feldspar alteration by disequilibrium CO_2-H_2O fluids in reservoir sandstones: implications for CCS

Natalie J. C. Farrell[1], Lining Yang[2], Michael J. Flowerdew[3], Chris Mark[4,5], Buhari Ardo[1], Kevin G. Taylor[1], Nico Bigaroni[1], Michael Pointon[3], Lewis Hughes[1], John Waters[1], and Lee Paul[1]

[1]Department of Earth and Environmental Sciences, Williamson Building, University of Manchester, Manchester, United Kingdom
[2]Institute of Marine Sciences (CNR-ISMAR), Bologna, Italy
[3]CASP, Cambridge, United Kingdom
[4]Department of Geology, Swedish Museum of Natural History, Stockholm, Sweden
[5]School of Earth Sciences, University College Dublin, Ireland

Correspondence: Natalie J. C. Farrell (natalie.farrell@manchester.ac.uk)

Received: 9 September 2025 – Discussion started: 22 September 2025
Revised: 23 January 2026 – Accepted: 26 January 2026 – Published: 5 March 2026

Abstract. Understanding how the minerals in reservoir rocks respond to CO_2 injection is vital for the success and safety of Carbon Capture and Storage (CCS) projects. Feldspars are the most common mineral in the Earth's crust and act as primary framework grains in sandstones. Compared to quartz, feldspars are mechanically weak and chemically reactive. Dissolved feldspars can re-precipitate as clays, which in CCS reservoirs could impact fluid-flow. While caprock mineral stability is well studied, reservoir mineral reactivity, particularly of feldspars, remains understudied. To address this knowledge gap, we present microstructural and geochemical data from batch experiments that reacted CO_2-enriched fluids with feldspar-bearing sandstone sampled from the Captain Sandstone Member, the primary reservoir for the Acorn CCS Project (UK).

Experiments were conducted in a hydrostatic pressure vessel at 70 MPa confining pressure, 50 MPa pore pressure, and temperatures ranging from 80 to 550 °C, using CO_2-enriched water to simulate reservoir conditions. Pre- and post-reaction samples were analysed using XRD, SEM-EDS, and XCT to assess microstructural and mineralogical changes. Results show that CO_2 : feldspar interactions differ significantly from control experiments involving water alone. At reservoir-relevant temperatures (80 °C), incongruent dissolution of K-feldspar weakened grains which led to microfracturing. At 250 °C, CO_2 fluids caused total dissolution of calcite grains and cement and selective leaching of calcium from oligoclase, enriching the pore fluid with Ca^{2+}. Above 400 °C, coupled dissolution–precipitation processes were observed, including congruent K-feldspar dissolution, secondary porosity development, and localised precipitation of Ca-aluminosilicates and K-bearing phases around dissolving K-feldspars. These transformations could alter reservoir flow pathways and induce mechanical risks, i.e. destabilising nearby faults or initiating reservoir collapse. Given feldspars' prevalence in crustal rocks and CCS sandstone reservoirs, their reactive behaviour under in-situ conditions and in the presence of aggressive fluids demands greater attention.

1 Introduction

Carbon Capture and Storage (CCS) projects aim to moderate the impacts of climate changes by injecting supercritical CO_2 into porous rock, such as deep saline aquifers and depleted hydrocarbon sandstone reservoirs, where it is intended to be stored for 10 000 years/indefinitely (IPCC, 2005). The productivity and safety of CCS projects hinge on our ability to efficiently flow CO_2 fluids into subsurface rock formations while preventing leakage. A key challenge for success is the ability to predict dynamically changing fluid-flow during injection and CO_2 plume migration (Juanes et al., 2006; Benson and Cole, 2008; Ringrose, 2020; Akhurst et al., 2025). This requires both a specific knowledge of the

pre-injection micro-scale reservoir properties, e.g., pore volume, pore connectivity, grain texture, and a broader empirical understanding of how injected fluids might mechanically and/or chemically alter this microstructure and thereby impact CCS project efficiency and safety (Rochelle et al., 2004; Hall et al., 2015; Rathnaweera et al., 2015; Shogenov et al., 2015; Fuchs et al., 2019; Foroutan et al., 2021; Pessu et al., 2025). Experimental studies have explored these CO_2-fluid-sandstone interactions showing that the acidic brines created by dissolution of CO_2 into formation fluids enhances dissolution of carbonate minerals, primarily as cements in sandstone reservoirs (Ross et al., 1982; Bertier et al., 2006; Hangx et al., 2015) with fewer studies reporting CO_2 fluid alteration of reactive aluminosilicates, including feldspars (Bertier et al., 2006; Hall et al., 2015; Lu et al., 2013). Geochemical models indicate that feldspar alteration may result in precipitation of carbonate minerals e.g., dolomite and dawsonite, which could permanently "lock-in" CO_2 (Durst and Vuataz, 2000, Seisenbayev et al., 2023). Feldspar : CO_2 reactivity could substantially influence the performance and stability of CCS reservoirs, yet their response to saturation with CO_2-enriched fluids under reservoir conditions (temperature *and* stress), including reaction types and rates and the consequences of reactivity, is poorly understood (Lu et al., 2013). This is a key knowledge gap especially in polymineralic rocks like sandstone where coupled chemical–mechanical processes are already poorly constrained.

1.1 Feldspar solubility

Feldspars are a volumetrically significant, mechanically weak and chemically reactive framework mineral in sandstones (Tullis and Yund, 1977) and most crustal rocks. In comparison to quartz, feldspars are highly reactive (Knauss and Wolery, 1986; Dove and Crerar, 1990). They can dissolve creating significant secondary porosity (Farrell and Healy, 2017) and re-precipitate as clays, which impede fluid-flow and mechanically weaken rocks (Farrell et al., 2021; Summers and Byerlee, 1977; Collettini et al., 2019, respectively), outcomes that could compromise both CCS reservoir efficiency and mechanical integrity. Feldspar solubility is strongly influenced by pH, as demonstrated in early experimental studies (Correns, 1961; Wollast, 1967). These investigations established that feldspar dissolution rates increase significantly under acidic conditions due to enhanced hydrolysis of Si–O and Al–O bonds in the crystal lattice, the rate of which is determined by grain surface area (Helgeson et al., 1984). Feldspars are mineralogically well defined, but their subsurface behaviour is uncertain. As key framework minerals in many of Earth's oldest crustal rocks e.g., gneisses, granites and sandstones, they can preserve evidence of their extensive geological histories (e.g. weathering, transport, burial, fluid interaction), which are reflected in their diverse microstructural textures and chemical heterogeneity. This inherited heterogeneity directly affects their reactivity. Across kilometre-scale reservoirs, their solubility can differ significantly based on provenance (detrital sources) and their burial or fluid-flow history (Glasmann, 1992), making some grains more or less prone to dissolution. Chemical alteration has been shown to enhance stress-corrosion cracking in quartz (Scholz, 1972), hence deformation of more reactive feldspars (via chemical dissolution and mechanical cracking) in the presence of chemically active CO_2 fluids is expected.

1.2 Predicting feldspar reaction rates

Mineral reaction rates are typically defined by experiments on powdered rock samples (Brantley et al., 2008). While using powders allows for control over reactant surface area, this method fails to account for the grain-to-grain stresses present in subsurface rocks. Even in hydrostatic experiments, such stresses at the grain scale can significantly accelerate mineral dissolution rates, often exceeding predictions based on powder-derived rate laws (Rutter, 1976; Wheeler, 1991). Considering the inherent weakness of feldspars under pressure-temperature conditions in the shallow crust, these stresses could induce microfracturing, which increases surface area and exposes fresh reactive surfaces that drive further reaction. Geochemical simulations frequently oversimplify feldspars, disregarding their diverse chemical compositions and variable textures i.e., surface areas, which are crucial for accurate reaction rate predictions (Helgeson et al., 1984). Enhanced understanding of feldspars, from quantifying the compositional variability in target reservoirs, to empirical evidence of feldspar : CO_2-reactions i.e., dissolution rates and secondary mineral formation, should improve the accuracy of geochemical and reactive transport models. We hypothesise that injection of CO_2 enriched fluids will impact the solubility of *stressed* feldspar grains and potentially alter the properties of sandstone CCS reservoirs, specifically the pore volume, pore connectivity, permeability and geomechanical stability.

This paper presents microstructural insights from a suite of coupled chemical : mechanical reaction experiments on feldspar-bearing sandstones from the Early Cretaceous Captain Sandstone Member from the Moray Firth, Scotland, the target reservoir for the Acorn CCS Project (Alcalde et al., 2019), highlighting the impact of CO_2 fluid saturation on reactive framework grains under subsurface conditions. In this study we used an externally heated, hydrostatic pressure vessel to investigate the solubility of various feldspars in a CO_2 saturated sandstone under hydrostatic stress, simulating CCS reservoir conditions in closed batch system experiments. Experiments were conducted at a range of increasing temperatures, effectively accelerating reaction rates simulating mineral reactions over hundreds of years – aligning with the timescales required for CO_2 storage. The temperature dependence of mineral dissolution follows an Arrhenius relationship, linking the reaction rate constant to temperature. For K-feldspar, the baseline rate constant is well-established,

and we approximate its temperature dependency using established rate laws for dissolution in varying pH fluids (Helgeson et al., 1984; Blum and Stillings, 1995). Unlike previous Captain Sandstone experimental studies that focused solely on reservoir mechanical stability using water as a pore fluid at ambient temperatures (Allen et al., 2020) or on the mechanical impact of CO_2 fluids on carbonate cement dissolution at low temperatures in an open pore fluid system (Hangx et al., 2015), this research explores the role of CO_2 fluid chemistry on the dissolution and stress-induced deformation of arguably more important *framework* grains over geological timescales. These results address a major knowledge gap in CCS reservoir appraisal and have scope to provide empirical constraints for long-term CO_2 containment predictions.

2 Material and Methods

This study used an overlapping programme of experimental rock deformation, microstructural and geochemical analysis to characterise the range/integrity of feldspars contained in a CCS target sandstone samples in the context of the reservoir geological history; experimentally assess how feldspars interact with CO_2-enriched fluids under subsurface conditions (temperature, pressure and grain scale stress) and consider the effect of feldspar dissolution and subsequent precipitation of clay minerals on reservoir properties of fluid-flow and mechanical strength. The characterisation of pre-experiment, in situ Captain Sandstone feldspars is summarised in Sect. 2.1 and reported along with a compositional analysis and a provenance model for direct and recycled feldspars by Flowerdew et al., 2024.

2.1 Material

Core plugs used in these experiments were taken from two sites within the historic petroleum well (14/29a-5, Goldeneye Field, around 8500 ft/2590.8 m), specifically from the D sand top and D sand middle intervals. These sandstones form the target "D sand" unit of the planned CO_2 storage reservoir at the Acorn CO_2 storage site, Scotland (Alcalde et al., 2019). The principal reservoir consists of fine to medium grained, high porosity, subarkosic turbidite deposits (Pinnock et al., 2003; Stewart and Marshall, 2020). Detrital mineralogy is dominated by quartz, plagioclase (albite and oligoclase) and orthoclase with some mica, glauconite and mudclasts. Some feldspars in the "D sand" subdivision of the Member have already been very reactive as shown by secondary porosity (Stewart and Marshall, 2020), more prominent at its top.

Captain Sandstone "D sand" samples comprise poorly cemented subarkose (Folk et al., 1970). Thin section analysis showed that grains are moderately to poorly sorted, 50 to $> 1000\,\mu m$ in diameter and loosely packed with around 30 % pore area. Intergranular pores are large and irregular or smaller and angular formed by the intersections of multiple rounded grains (Fig. 1A). X-ray diffraction analysis showed that samples broadly contain 76 % quartz, 8 % plagioclase, 8 % K-feldspar, 6 % clays, predominantly kaolinite plus minor amounts of 1 % calcite, 1 % glauconite (XRD method and results, Table S2 in the Supplement). Mineralogical makeup was also determined by using element data obtained from scanning electron microscopy energy dispersive X-ray spectroscopy (hereafter abbreviated to EDS) mapping overlain on Backscattered electron images (BSE) taken using a Scanning Electron Microscope (SEM) (Fig. 1B).

Captain Sandstone feldspars are mineralogically and texturally diverse showing three dominant mineralogies; two plagioclases, intermediate NaCa bearing oligoclase and end member Na-rich albite and K-feldspar (Fig. 2A–E). The reactivity of plagioclase is already apparent in the pre-experiment samples, as indicated by the skeletal texture of albite grains (Fig. 2B). This texture likely results from the albitisation of oligoclase, driven by chemical exchange where Ca in oligoclase is replaced by Na from brines, substituting Ca^{2+} ions with Na^{+}, and releasing Ca^{2+} into the fluid (Fig. 2C). Additionally, plagioclase reaction and dissolution (whether oligoclase or albite) has likely released Al and Si to form kaolinite precipitates during geological diagenesis (Fig. 2B and C). Both plagioclase and oligoclase grains commonly range between ~ 100–$200\,\mu m$ diameters and display blocky, subrectangular grain boundaries with rounded edges (Fig. S3 in the Supplement). K-feldspars tend to be larger than plagioclases, averaging 200–300 µm diameter and display coherent, rounded grain boundaries abutting similarly shaped quartz grains (Fig. 2C). Many K-feldspars show perthite textures with darker fine bands and streaks of albite lamellae oriented along cleavage planes (Figs. 2D and S3). Some K-feldspars show reaction in perthite grains with some preferential dissolution of albite lamellae and opening up of intergranular porosity along these features (Fig. 2F).

2.2 Experimental method

Eight reaction experiments were performed on 9.5 mm diameter core plugs of Captain Sandstone Member "D sand" using hydrostatic pressure vessels at ~ 70 MPa confining pressure (Pc) aka ~ 3 km burial depth with 50 MPa pore fluid pressure (Pf). Four experiments used CO_2 saturated water as a pore fluid (as a proxy for CO_2 injection), while four control experiments used H_2O under the same conditions. We experimentally modelled the progression of feldspar reactivity under subsurface conditions by conducting experiments across a range of temperatures (from 80 °C, aka reservoir conditions, up to 550 °C), using elevated temperatures as a proxy for longer reaction time. This approach uses the Arrhenius equation, which describes the temperature dependence of reaction rates, allowing higher temperatures to accelerate mineral reactions and simulate longer-term geochemical processes within practical and repeatable laboratory timescales (calculated reaction rate ratios for these experiments detailed in the

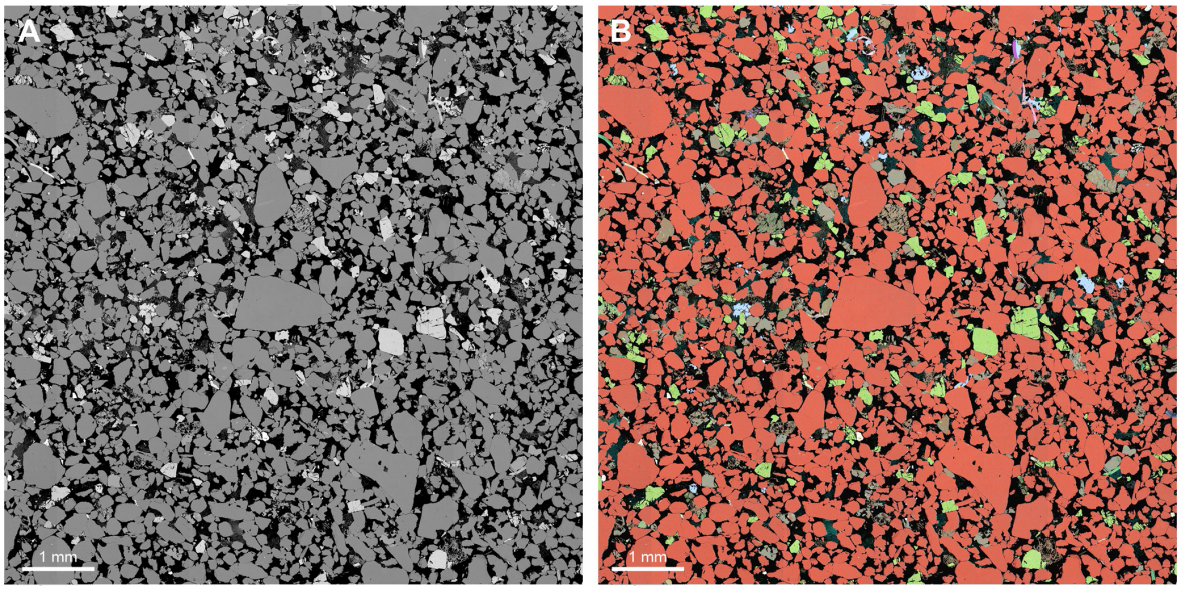

Figure 1. Back scattered Electron and semi-transparent EDS elemental maps of pre-experiment D sand, Captain Sandstone (**a** and **b**, respectively). Black = pore/void space, red/orange = quartz, green/yellow = orthoclase, grey/brown = oligoclase, pale blue = calcite

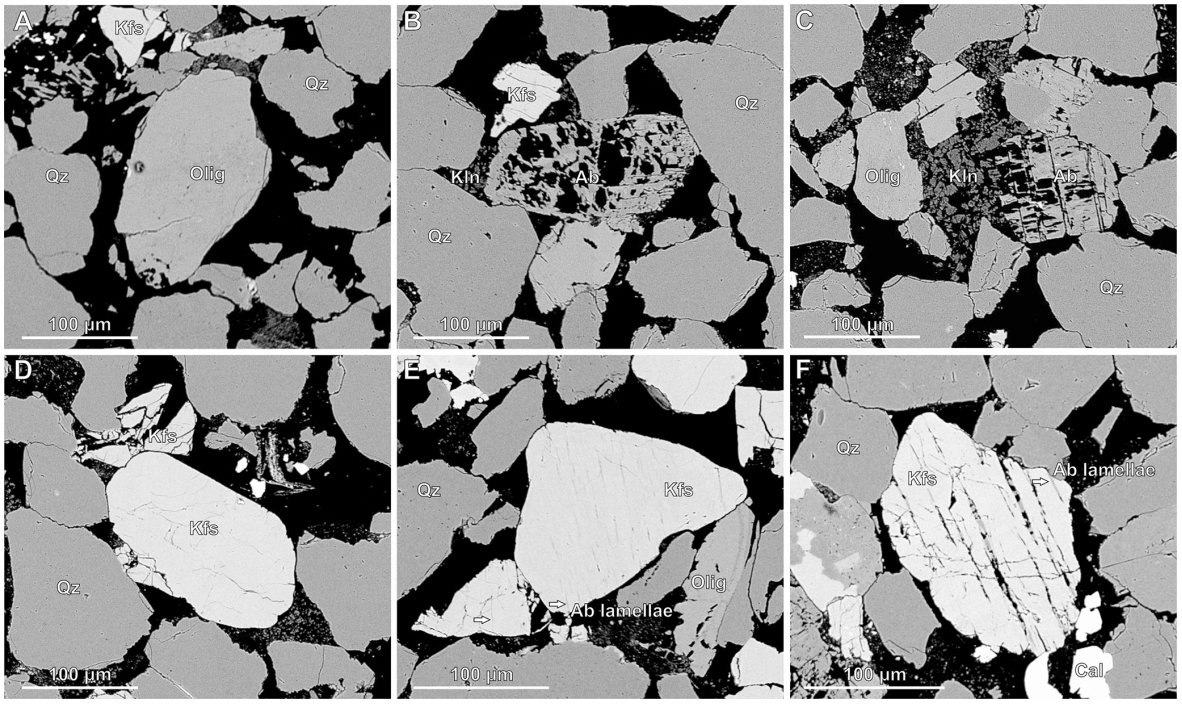

Figure 2. Back Scattered Electron images showing feldspar types including plagioclases, oligoclase **(A, C)** and albite **(B, C)** and K-feldspar **(D–F)** in pre-experiment samples of Captain Sandstone. Abbreviations follow Whitney and Evans, 2010. Quartz (Qz), (Oligoclase (Olig), K-feldspar (Kfs), Albite (Ab), Kaolinite (Kln).

Supplement). These results can then be extrapolated to reservoir temperatures following standard practice in mineral-reaction studies (Blum and Stillings, 1995), a methodology commonly used to model reservoir evolution over geological timescales (Brantley et al., 2008; Hangx and Spiers, 2009; Hellmann et al., 2012). Experimental conditions are detailed in Table 1.

Experiments were conducted using externally heated triaxial deformation apparatus, "Nimonic 2" and "Nimonic 3". The pressure vessel and sample assembly in these rigs

Table 1. Experimental conditions for batch reactor tests conducted in triaxial deformation rigs "Nimonic 2" and "Nimonic 3". Core plugs of Captain Sandstone were reacted with differing pore fluid chemistries under constant Pf, Pc and temperatures for durations of 6–10 d with the objective of assessing the influence of pore fluid chemistry and temperature on mineral stability and microstructure.

Sample ID	Rig ID	Pore fluid chemistry	Temperature (°C)	Confining pressure (MPa)	Pore fluid pressure (MPa)	Duration (days)
Dt02	Nimonic 3	H_2CO_3	80	70	50	6
Dm07	Nimonic 2	H_2O	80	70	50	6
Dt01	Nimonic 3	H_2CO_3	250	70	50	10
Dm04	Nimonic 2	H_2O	250	77	50	10
Dt03	Nimonic 3	H_2CO_3	400	70	50	6
Dm06	Nimonic 2	H_2O	400	75	50	6
Dm01	Nimonic 3	H_2O	550	72	50	6
Dm05	Nimonic 3	H_2CO_3	550	80	50	6

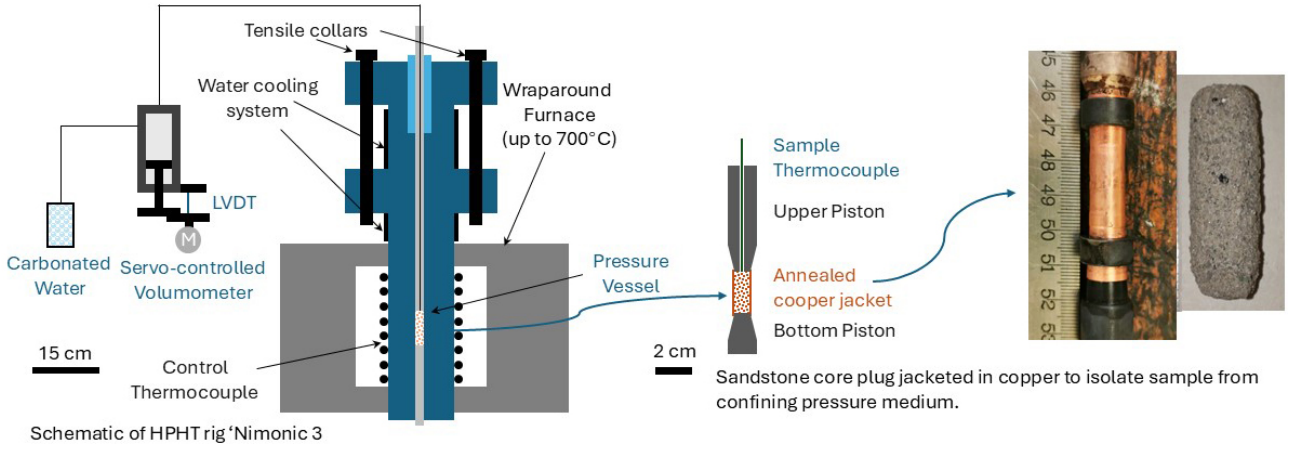

Figure 3. Schematic cross section diagram of high pressure, high temperature triaxial rig "Nimonic 3" illustrating the sample assembly within the Nimonic pistons (rhs), confinement of sample with the pressure vessel and furnace (centre) and pore volumometer controlling injection and pressure of pore fluid along the top piston (lhs).

are constructed from nickel alloy (Nimonic®115) which is highly resistance to oxidation and compatible with carbonic acid and other corrosive fluids at elevated temperatures, preventing piston reactions that could contaminate the rock sample (Fig. 3). Samples were contained within annealed copper jackets to isolate them from the water confining fluid, which was pressurised to reservoir conditions using a compressed air pump. Both Pc and Pf were gradually increased in succession up to the required experiment conditions to prevent pore collapse and preserve the starting material grains and microstructure. For control experiments, the pore fluid was tap water (very soft with total hardness of $16\,mg\,L^{-1}$, Table S1), while for CO_2 proxy experiments, the same water was saturated with CO_2 using a SodaStream®. The resulting "fizzy water" contained $\sim 6\,g\,L^{-1}$ CO_2, yielding a pH of 4. Pf was controlled using a pore volumometer with a piston driven by a DC servo-motor. This system allowed precise adjustments of the piston in and out of a $3\,cm^3$ pressure vessel to maintain a constant Pf through feedback control from a pore pressure transducer. A 50 MPa Pf was used in all experiments to ensure that water remained in a liquid state even above its critical point $\sim 400\,°C$, thereby preserving consistent stress conditions throughout the experiments. Once at pressure, the experiment temperature was applied using upper and lower external furnaces which create a thermal gradient which can be used to position a "hot spot" within the pressure vessel focused around the relatively small sample. The furnace temperature was increased to the required level using variacs, which control the voltage to the furnaces for precise adjustments. The temperature was then maintained at the set value for 6 d with stable power regulation from the variacs. Sample temperature was monitored using an inconel-sheathed thermocouple inserted down the upper piston. Pre experiment calibrations showed a temperature range of $< 2\,°C$ along the sample length at 500 °C. Experiments were ended by decreasing temperature back to ambient conditions then unloading the Pf and Pc in tandem and in reverse to protect the pore space.

2.3 Microstructural analysis

Post experiment jacketed core plugs were injected with epoxy under a vacuum and then halved to make thin sections covering the central portion of the sample cylinder. Polished sections were carbon coated before being imaged using a Zeiss Evo MA 15 scanning electron microscope housed at CASP. Back scattered electron (BSE) images and elemental maps were collected using one or a combination of a Zeiss Back Scatter Electron (BSE) detector, an Oxford Instruments Ultim Max 100 Energy dispersive x-ray spectrometer (EDS) detector and an Oxford Instruments Unity detector. Montages of images that cover the thin section were collected at 20 kV and 2000 pA probe current, and 10 kV and 200 pA probe current where greater definition imagery was required. Images and data were collected, manipulated and exported using Oxford Instruments AZtec software version 6.1, coupled with the AutoPhaseMap and AZtecFeature analysis and CASP's in-house mineral classification scheme.

Microstructural analysis was conducted on BSE and EDS images of pre- and post-experiment thin sections to examine and characterise mineral phases and textures and analyse reaction pathways between grains. This analysis was facilitated by the generation of EDS x-ray spectra for specific points or regions on the map. Post experimental mineral dissolution and/or precipitation was quantified from BSE maps overlain with semi-transparent EDS maps by thresholding the area covered by key mineral phases (K-feldspar, plagioclase, calcite) using image analysis software ImageJ and defining this result as a percentage of the total grain content (see Sect. S1.4 in the Supplement, for more information). Individual montage images were analysed separately to investigate the heterogeneity of pore and grain distributions (as per method in Farrell and Healy, 2017). Additional 3D micro-CT images were produced of pre and post experiment samples to assess grain deformation and pore networks. The micro-CT data had limited resolution compared to the SEM data and so are not discussed here but are included in the Supplement.

3 Results

Microstructural and compositional changes were identified in all experimentally reacted samples indicating cation exchange between pore fluid and sandstone samples after experimental run times of 6 d. The experimental duration, stress conditions and pore fluid compositions are summarised in Table 1. In this section we present petrographic results for specific mineral phases and their alteration in the presence of CO_2-enriched water compared with H_2O (i.e. tap water) (Figs. 4–10). Image analysis was used to quantify the extent of mineral alteration in post-experiment samples compared to pre-experiment. Mineral quantifications are presented as box plots to show changes in mean mineral content which could be used in geochemical models and to illustrate the statistical distribution and variability of mineral grains within samples, highlighting dissolution heterogeneity (Fig. 1). Additional microstructural data from all experiments are shared in the Supplement.

3.1 Alteration of K-feldspar

3.1.1 K-feldspar : CO_2 enriched pore fluids

Post-experiment BSE imaging reveals significant microstructural changes in K-feldspar grains reacted at different temperatures. Compared to pre-experiment samples, which exhibit minimal fracturing (Figs. 2D–F and S3), post-experiment K-feldspar grains display dissolution, systematic microfracturing and grain fragmentation and development of secondary porosity providing evidence of active mineral alteration during experiments (Figs. 4, S5–S8).

At 80 °C, open pores develop on grain surfaces as linear and parallel "cracks" or "seams" that propagate into grain interiors at high angles, often forming bimodal cross-cutting sets aligned with cleavage planes (Figs. 4A and B, S5 and S6) and commonly oriented with albitised lamellae (Fig. 5A). Some tightly packed K-feldspars are fractured against adjacent grains and crushed between quartz grains, which remain largely intact, suggesting mechanical weakening of stressed K-feldspars, likely enhanced by localised dissolution and development of porous "seams" on the grain edges (Fig. S5). At 250 °C intergranular dissolution becomes more pronounced, suggesting that increased intergranular fracture density both enhanced reactive surface area and created conduits for further fluid-rock interaction (Fig. 4C). At 400 °C, K-feldspar dissolution is accompanied by the formation of thin (~ 3 µm), discontinuous calcic aluminosilicate overgrowths along open grain boundaries, particularly around smaller K-feldspar fragments (Figs. 4D and 5B). EDS spot analysis shows overgrowths are chemically equivalent to calcic plagioclase (andesine- anorthite) (Fig. S17). At 550 °C, intergranular fractures widen (5–10 µm vs. < 5 µm at 400 °C), and K-feldspars are segmented by cross-cutting fractures into fragments with rounded, dissolution-modified edges (Fig. 4E and F). In this sample secondary porosity is widespread and these pores can often be identified by "ghosts" of former grain outlines defined by secondary clay precipitates (Figs. S6–S8 and XCT images and animations, https://doi.org/10.6084/m9.figshare.30061294.v1, Farrell et al., 2025).

Secondary precipitation phases are most prominent at higher temperatures (400–550 °C), appearing as a Ca-rich pale blue and K-rich bright green phases in combined EDS-BSE images (Fig. 5). Precipitates are often located around "free" edges of grains i.e. not in contact with adjacent grains and become thicker (~ 10 µm) and more continuous at 550 °C, while grain to grain boundaries display concave-convex contacts with adjacent quartz grains, implying differential dissolution and possible influence of intra-

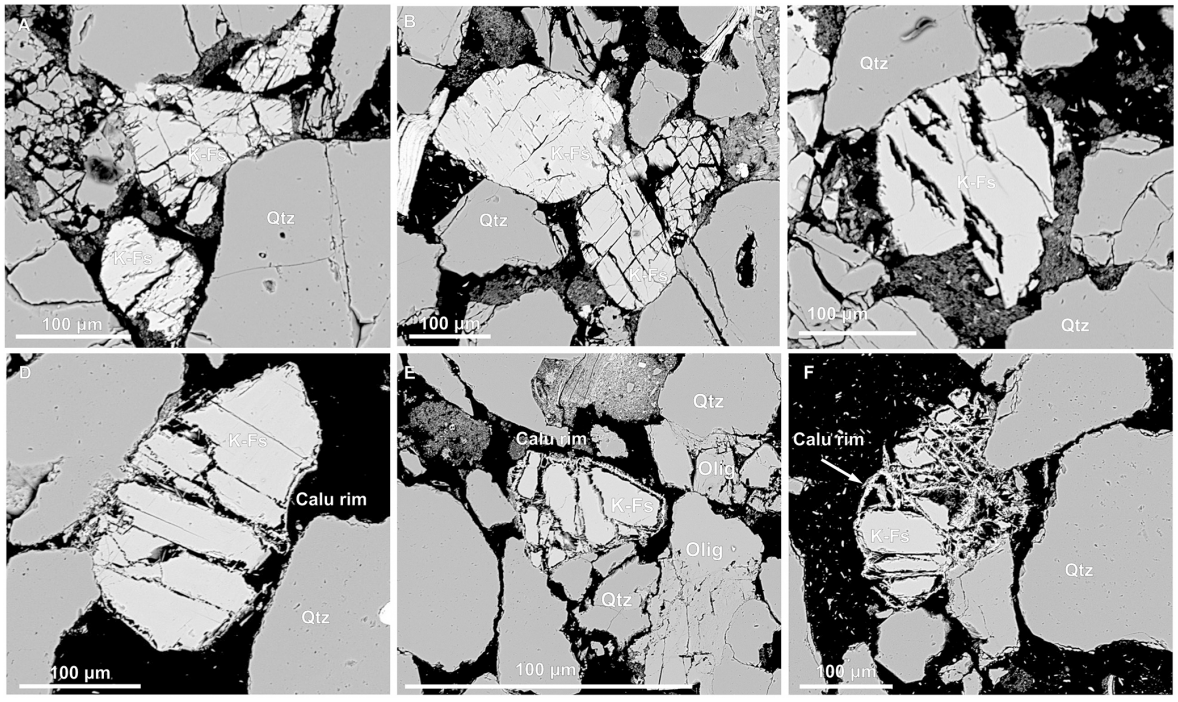

Figure 4. Back scattered electron (BSE) images showing progressive K-feldspar (Kfs) alteration via chemical and mechanical deformation with increasing temperature reaction experiments conducted with CO_2 fluids at hydrostatic conditions, including – dissolution and grain microfracturing at experiments conducted at 80 °C **(A, B)**, grain dissolution at 250 °C **(C)**, and secondary mineral growth around K-feldspar grains at 550 °C **(D–F)**. Quartz (Qz), (Oligoclase (Olig), K-feldspar (Kfs), Calcic aluminosilicate (Calu).

granular stress on reactivity (Fig. 5C). Dissolved K-feldspar grain edges typically exhibit irregular, serrated morphologies (Figs. 5D, S7 and S8). In some images, a narrow void separates receding K-feldspar grain edges from calcitic overgrowths, marking a zone where dissolution likely outpaced precipitation (Figs. 4D–F and 5c, d). High-magnification imaging shows outward nucleation of these calcic aluminosilicates at high angles from K-feldspar surfaces and aligned crystallographically with the host grain (Fig. 5D). Thin K-feldspar strands remain linked to the overgrowths, suggesting ongoing elemental exchange. A K-rich phase, likely mica, is also observed as a bright green band within and beyond the pale blue rims, forming spindly, fibrous morphologies (Fig. 5D). In the high temperature experiments, the K-rich phase is also precipitated in pore space and pore throats, within the clay masses small crystals of the calcic aluminosilicate has nucleated (Fig. 5B).

3.1.2 K-feldspar : H_2O pore fluids

In H_2O experiments (tap water as pore fluid), post-reaction samples show temperature-dependent microstructural changes distinct from those observed under CO_2-enriched fluid conditions. At 80 °C, microfractures in K-feldspar are primarily grain-bound, with curvilinear to subparallel orientations (Fig. 6C and D), the latter suggesting crystallographic control and possible mechanical weakening. These features differ from the chemically driven dissolution seams, serrated grain edges, and widening of intragranular fractures observed in the CO_2 experiments (Sect. 3.1.1). At higher temperatures 400 °C, K-feldspars appear to have been mechanically weakened with post experiment samples showing enhanced intergranular fracturing, local grain crushing, and some convex–concave grain contacts. At 550 °C, K-feldspars in H_2O experiments exhibited irregular intergranular fracturing and precipitation of calcic aluminosilicate overgrowths and a K-rich phase which also formed discontinuous rims around grain edges (Figs. 6, S9–S12). However, unlike the CO_2 experiments, these rims are thinner and more spatially limited, and K-feldspar dissolution features were less pronounced. These contrasts highlight the influence of pore fluid chemistry on K-feldspar enhanced reactivity under CO_2-enriched conditions.

3.2 Alteration of plagioclase

3.2.1 Plagioclase : CO_2 enriched pore fluids

The Captain Sandstone Member contains two types of plagioclase: Na-rich end member albite and intermediate oligoclase (Fig. 2). The impact of CO_2 enriched pore fluids on oligoclase and albite, is markedly different to each other. At 80 °C (reservoir temperature) albite grains remain coherent/intact with their original grain boundaries and skeletal tex-

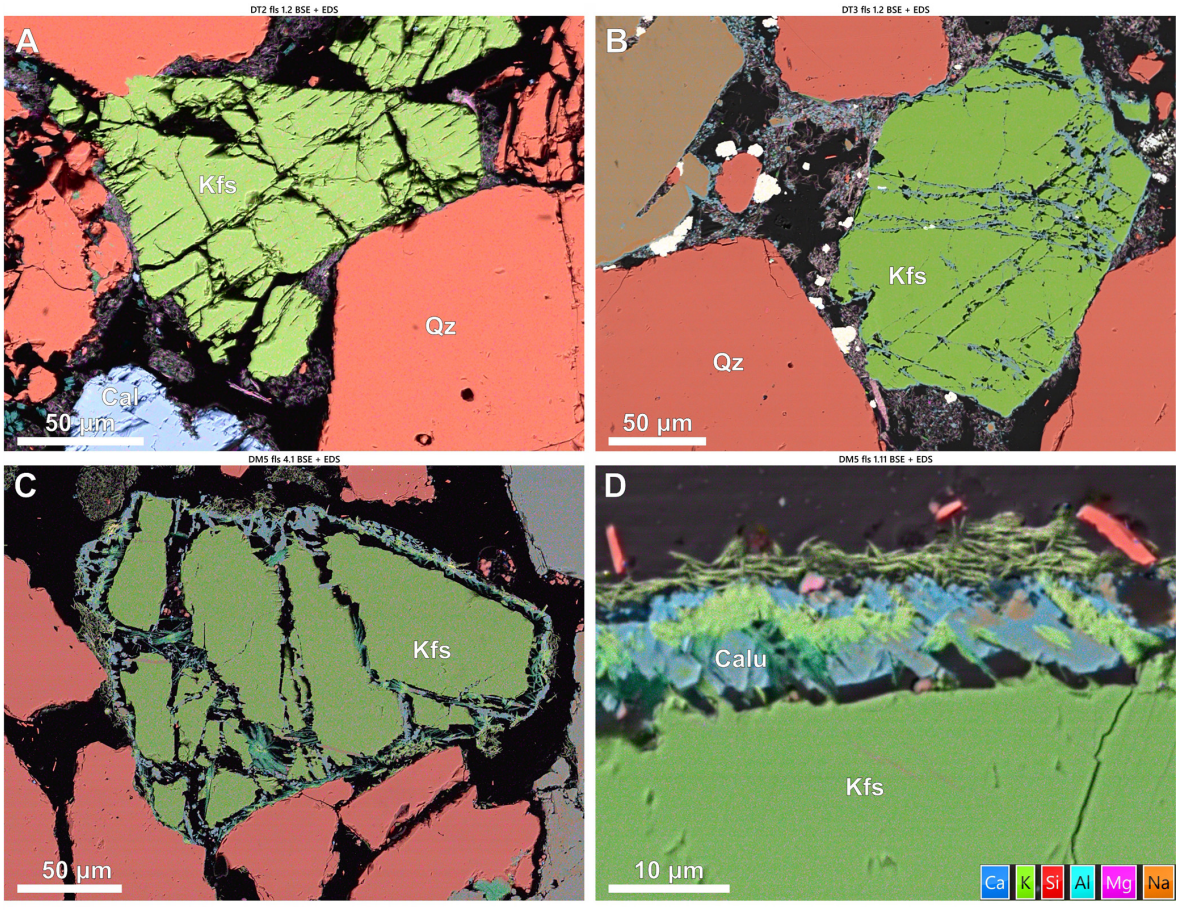

Figure 5. High-magnification backscattered electron (BSE) images, overlaid with semi-transparent elemental EDS maps, showing progressively enhanced microfracturing, dissolution, and secondary precipitation in K-feldspar saturated with CO_2 enriched fluids at a range of experimental temperatures (80 °C **(A)**, 400 °C **(B)**, and 550 °C **(C, D)**.

tures (Fig. 7A) while oligoclase grains show minor marginal dissolution or "scalloping" along grain edges (Fig. 7B). At 250 °C, oligoclase grains have complex, indented grain boundaries often surrounded by kaolinite and mixed-element fine clays (Fig. 7B and C). Some grains show evidence of intergranular pore development or surface etching, though intergranular microfracturing is limited or absent. At higher temperatures (> 400 °C), intergranular porosity in oligoclase increases due to grain dissolution (Fig. 7E and F). Albite grains also show significant intergranular porosity, though this appears consistent with the skeletal textures observed in pre-experiment sandstones (Fig. 7D).

Combined BSE and EDS images or oligoclase grains reacted at 400 °C show leaching of Ca+ from grain edges leaving an original Na-Ca rich grain centre, a ∼ 20–30 µm thick Na rich albitic grain edge plus 2–5 µm calcium aluminosilicate rims similar to features observed on K-feldspar grains but without the void space between the dissolving host grain and secondary precipitate (Fig. 8). In contrast, albite shows minimal evidence of chemical interaction with CO_2-enriched fluids at any temperature (Fig. 7A and D).

3.2.2 Plagioclase : H_2O pore fluids

Experiments run with H_2O pore fluids show no obvious chemical alteration of albite or oligoclase at experiments conducted at 400 °C and below, but in these samples the oligoclase grains do show more intergranular fractures with many grains fractured along cleavage planes (Fig. 9A). At higher temperatures (550 °C) some oligoclase grains show chemical dissolution and "scalloping" of the grain boundary (Fig. S12) with few grains exhibit a thick, porous texture calcite overgrowths apparently tracking the original grain boundary as this boundary abuts the contact with quartz grains (Fig. 9E and F). In this sample calcite cements are still present as singular, isolated patches of cement (Figs. 10C and S13).

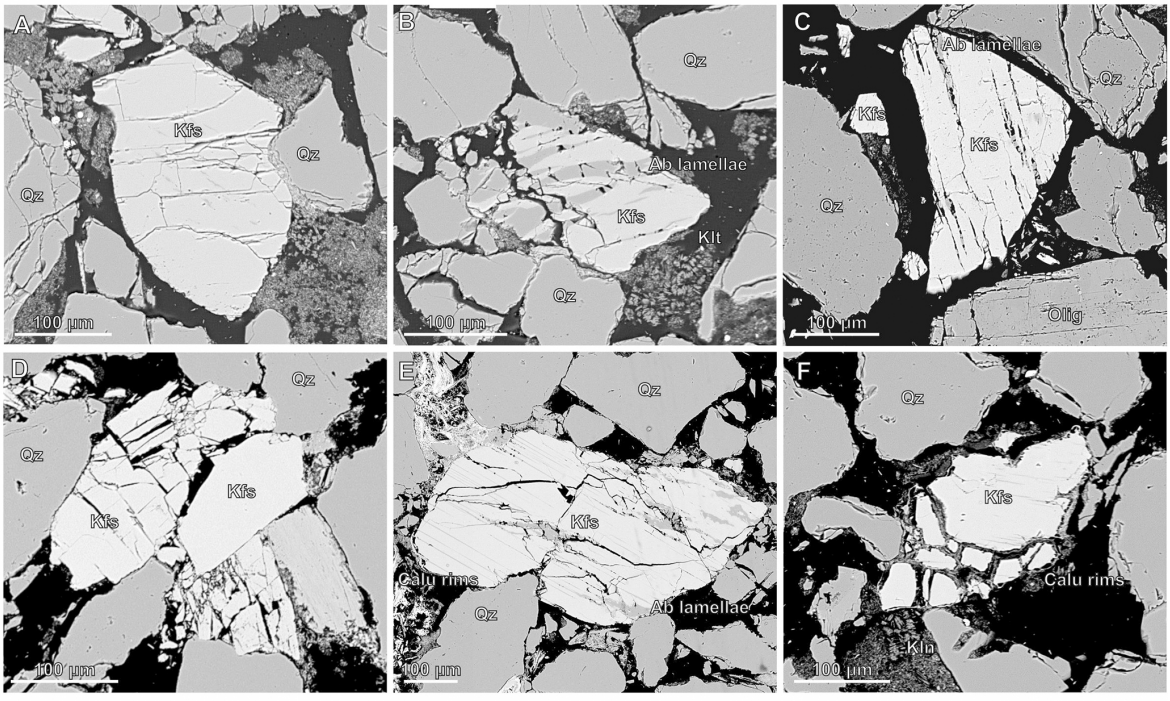

Figure 6. Back scattered electron images showing mechanical fracturing of K-feldspar grains in reaction experiments with H_2O pore fluid at 80 °C **(A, B)**, 250 °C and 400 °C **(C, D)** and 550 °C **(E, F)**. Fractures are generally grain bound with irregular, curvilinear traces and some crystallographic alignment at experiments conducted at higher temperatures **(C, E)** indicating mechanical weakening. Minimal K-feldspar dissolution and persistent presence of albite lamellae suggest reduced alteration under H_2O compared to CO_2-saturated conditions.

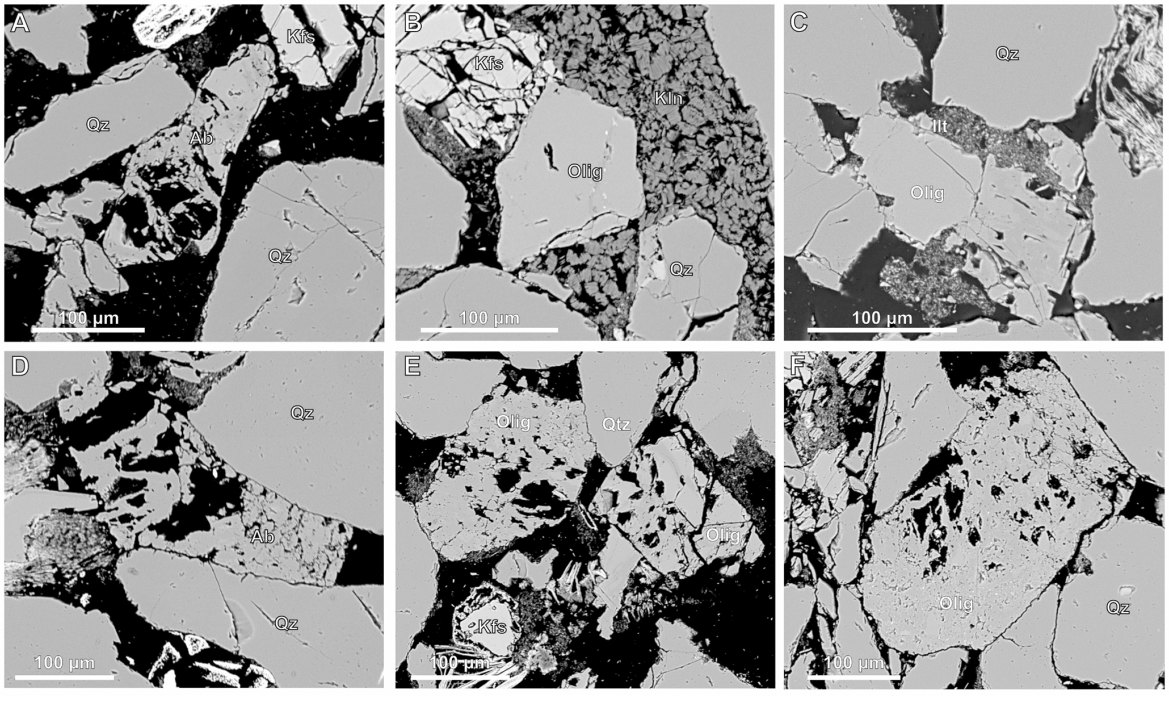

Figure 7. Back scattered electron (BSE) images showing plagioclase grains post reaction experiment condition with CO_2 enriched fluids. Images show no alteration of albite grains at 80 or 550 °C **(A, D)** while oligoclase grains appear partially dissolved on the grain boundaries at 250 and 400 °C **(C)** and etching and intergranular porosity at 550 °C **(E, F)**.

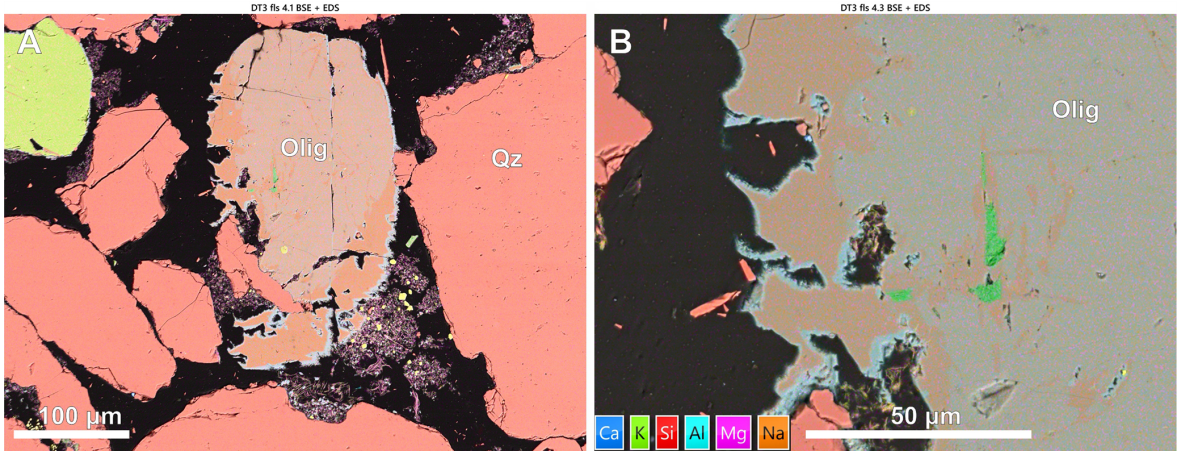

Figure 8. Back scattered electron (BSE) images with overlain EDS map showing grain boundary dissolution of oligoclase grains reacted with CO_2 fluids at 400 °C.

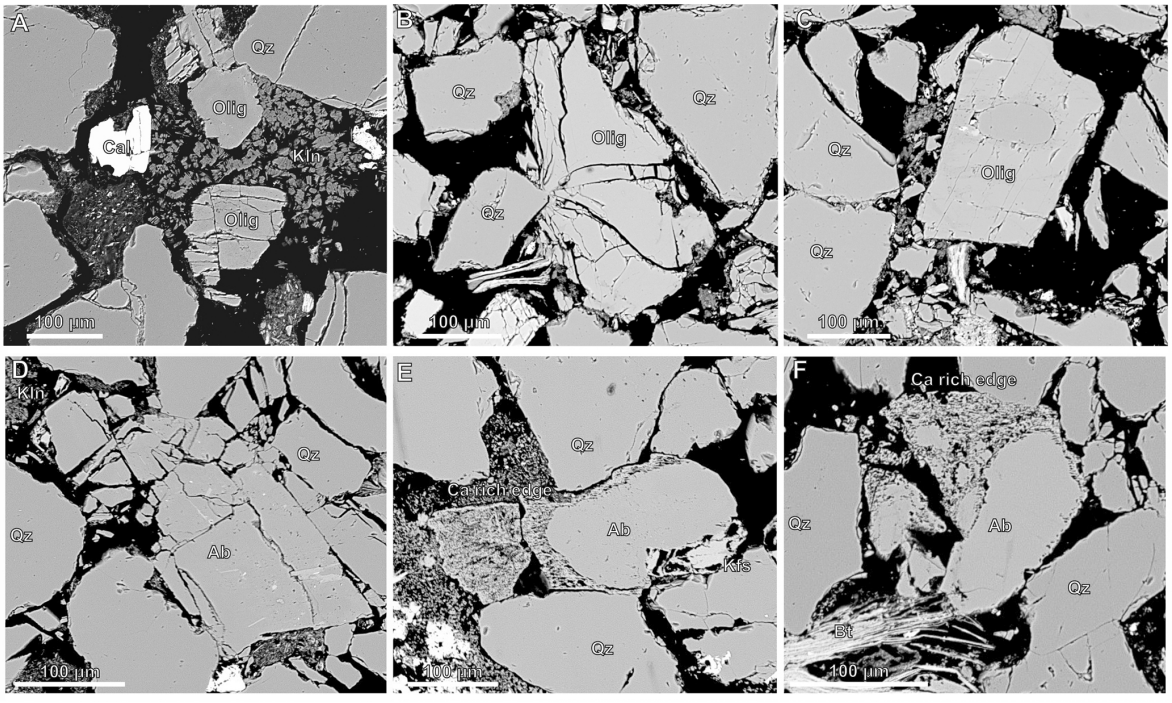

Figure 9. Backscattered electron (BSE) images of plagioclase feldspar grains (including both oligoclase and albite) following reaction with H_2O pore fluid. Images from 80 and 250 °C experiments **(A–C)** show enhanced mechanical fracturing with minimal evidence of chemical alteration. Albite reacted at 550 °C **(D)** also displays fracturing without signs of chemical dissolution. In contrast oligoclase grains reacted at 550 °C appear partially dissolved, with sodium leached from the grains, resulting in a calcite rich grain boundary presenting with a porous "mesh" texture **(E, F)**.

3.3 Dissolution of calcite grains and cement with CO_2 enriched water and H_2O pore fluids

Pre experiment samples recorded XRD analysis recorded around 1 % calcite which occurred as both grains and cement (Fig. S4). Following the experiments, calcite was nearly entirely removed in the CO_2 experiment samples, whereas it remained visible in post H_2O experiment samples (even at temperatures up to 550 °C) as grains and patches of cement (Fig. 10).

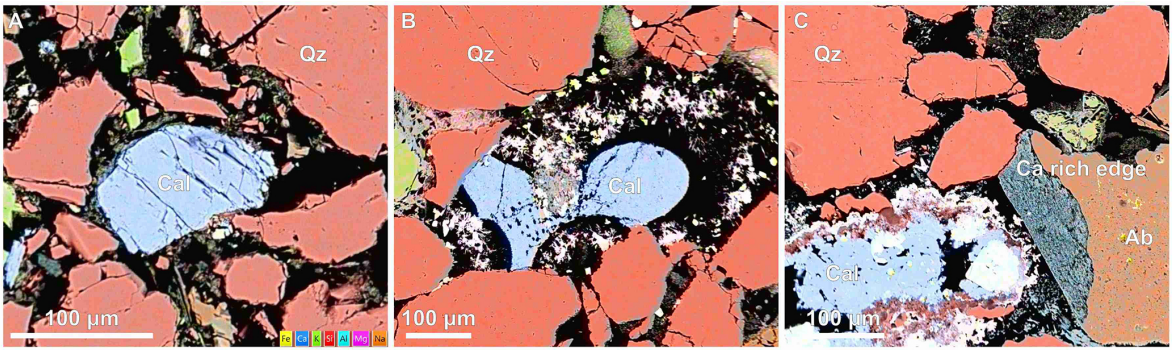

Figure 10. Back scattered electron images of calcite grains and calcite cement in post H_2O experiment samples reacted at 250 °C **(A)**, 400 °C **(B)**, 550 °C **(C)**.

3.4 Quantitative microstructural and mineralogical alteration

Image analysis was performed to quantify mineral alteration in both CO_2 and H_2O experiment samples. Specifically, changes in the 2D percentage of pore area and the key reactive minerals (K-feldspar, plagioclase, and calcite) were measured. To account for heterogeneity and spatial distribution, the percentage area of each mineral was quantified from multiple subsections of each thin section (between six and twelve 3 mm × 3 mm images per sample) following methodology used in Hall et al. (2015). The results are presented using box-and-whisker plots to illustrate the data spread and account for heterogeneity (Fig. 1). Two pre-experiment samples, "Dt" and "Dm", were analysed, each with slightly different pre experiment bulk rock compositions (see Table S2). Core plugs from the Dm sample were primarily used in H_2O experiments, while Dt sample core plugs were used in CO_2 experiments.

Image analysis revealed minimal changes in 2D pore area between pre-experiment samples, which averaged 29 % and 32 % pore area and post-experiment reacted with H_2O and CO_2 at 80 and 250 °C, which averaged 30 % and 32 %) (Fig. 1A). However, this decreased to 26 % pore area in samples reacted with H_2O and CO_2 at 400 °C and with H_2O 550 °C, possibly due to enhanced grain packing and pressure solution observed in images (Figs. 9E and S11) and secondary mineral precipitation, while samples exposed to CO_2 at 550 °C maintained pore areas over 30 % (Fig. 4A). This difference is likely due to additional secondary porosity produced by K-feldspar and calcite cement and grain dissolution (Fig. S8) as pressure solution and mineral precipitation are also observed in these samples (Fig. 7F and S7).

Boxplots show the percentage of reactive grains (K-feldspar, plagioclase, and calcite) expressed as their proportion relative to the total number of mineral grains visible in each image (Fig. 1B–D). The average proportion of K-feldspar grains decreased by nearly half in all samples exposed to H_2O and CO_2, with a more significant reduction observed in post CO_2 experiment samples (Fig. 1B). These CO_2 reacted samples also exhibited a more heterogeneous distribution of K-feldspar, as indicated by the wider interquartile ranges on the grey CO_2 box-and-whisker plots compared to the blue H_2O boxes, suggesting variable dissolution across the sample (Fig. 11B). Due to limitations in image thresholding, albite and oligoclase were grouped together under the category of "all plagioclase". In samples reacted with CO_2, the proportion of plagioclase decreased by approximately 25 %, indicating some dissolution. In contrast, H_2O-reacted samples show little change in plagioclase area (Fig. 11C). XRD analysis determined ∼ 1 % calcite in the pre-experiment samples (Table S1), observed in thin sections as carbonate clasts, bioclasts, and carbonate cement patches (Fig. S4). Quantitative image analysis showed low area fractions of calcite across many pre- and post-experiment images (0 %–0.9 %). Pre-experiment samples had median calcite area fractions of 0.2 % and 0.4 %, whereas post-experiment samples generally showed lower median values. In CO_2-reacted samples, calcite abundance decreased by more than half at 80 and 250 °C, with calcite nearly absent at 400 and 550 °C (Fig. 11D). In contrast, H_2O-reacted samples showed only a slight decrease at 80 °C, with calcite contents remaining largely unchanged at higher temperatures.

4 Discussion

4.1 Experimental reaction mechanisms and microstructural evolution

Microstructural analysis of reacted samples reveals a complex interplay of feldspar dissolution and secondary mineral precipitation in the presence of H_2O and CO_2-enriched pore fluids. These reactions are driven by deformation mechanisms such as diffusive mass transfer, including pressure solution, microfracturing, which generates fresh surfaces and increases reactivity, ion exchange and hydrolysis. Key contrasts between H_2O and CO_2 fluid experiments samples in-

https://doi.org/10.5194/se-17-407-2026

Table 2. Summary of observed chemical and mechanical alteration and interpreted reactions and deformation mechanisms from experiments reacting CO_2 enriched fluids with core plugs of Cretaceous Captain Sandstone "D sand" from the Acorn CCS field.

Experiment temperature (°C)	K-feldspar		Oligoclase		Albite	
	Chemical alteration	Mechanical deformation	Chemical alteration	Mechanical deformation	Chemical alteration	Mechanical deformation
	Localised incongruent dissolution producing grain-edge, cleavage-parallel porous seams; preferential release of K^+ ($\pm Na^+$, Ca^{2+})	Stress-assisted microfracturing and local grain crushing against quartz, enhanced by chemical weakening	Incongruent dissolution around grain boundary with early Ca^{2+} leaching creating scalloped edges	Grains largely intact with no micro-fracturing	Largely unaltered; skeletal textures preserved	Coherent, no microfracturing
250	Transition toward more congruent dissolution along microfractures, increasing reactive surface area	Intergranular microfracturing generating fresh reactive surfaces	Continued incongruent dissolution producing some intergranualar porosity and indented grain boundaries rimmed by kaolinite and mixed clays	Minor deformation with compaction and minor microfracturing	Largely unaltered	Coherent, no microfracturing
400	Coupled dissolution–precipitation (CDP) reaction during K-feldspar dissolution and precipitation of thin ($\sim 3\,\mu m$) calcic aluminosilicate rims and K-bearing clays via ion exchange (K^+–Ca^{2+})	Sets of through-going, cross-cutting micro-fractures possibly aligned along cleavage and/or chemically altered grain	Dissolution increases intergranular porosity by leaching of Ca^{2+} from edges leaving 20–30 µm Na-rich boundary and thin 2–5 µm Ca-rich rim	Limited micro-fracturing, fractures less pervasive than K-feldspar	Minimal chemical change	Coherent, skeletal textures maintained
550	Extensive congruent dissolution and grain comminution producing significant secondary porosity. Precipitation of thick ($\sim 10\,\mu m$) calcic aluminosilicate (anorthitisation) and K-clays	Concave–convex grain contacts with quartz indicating pressure solution	Continued dissolution and precipitation developing albitic rims and enhancing intergranular porosity	Minor pressure solution features at grain contacts	Largely unaltered	Coherent, skeletal textures maintained

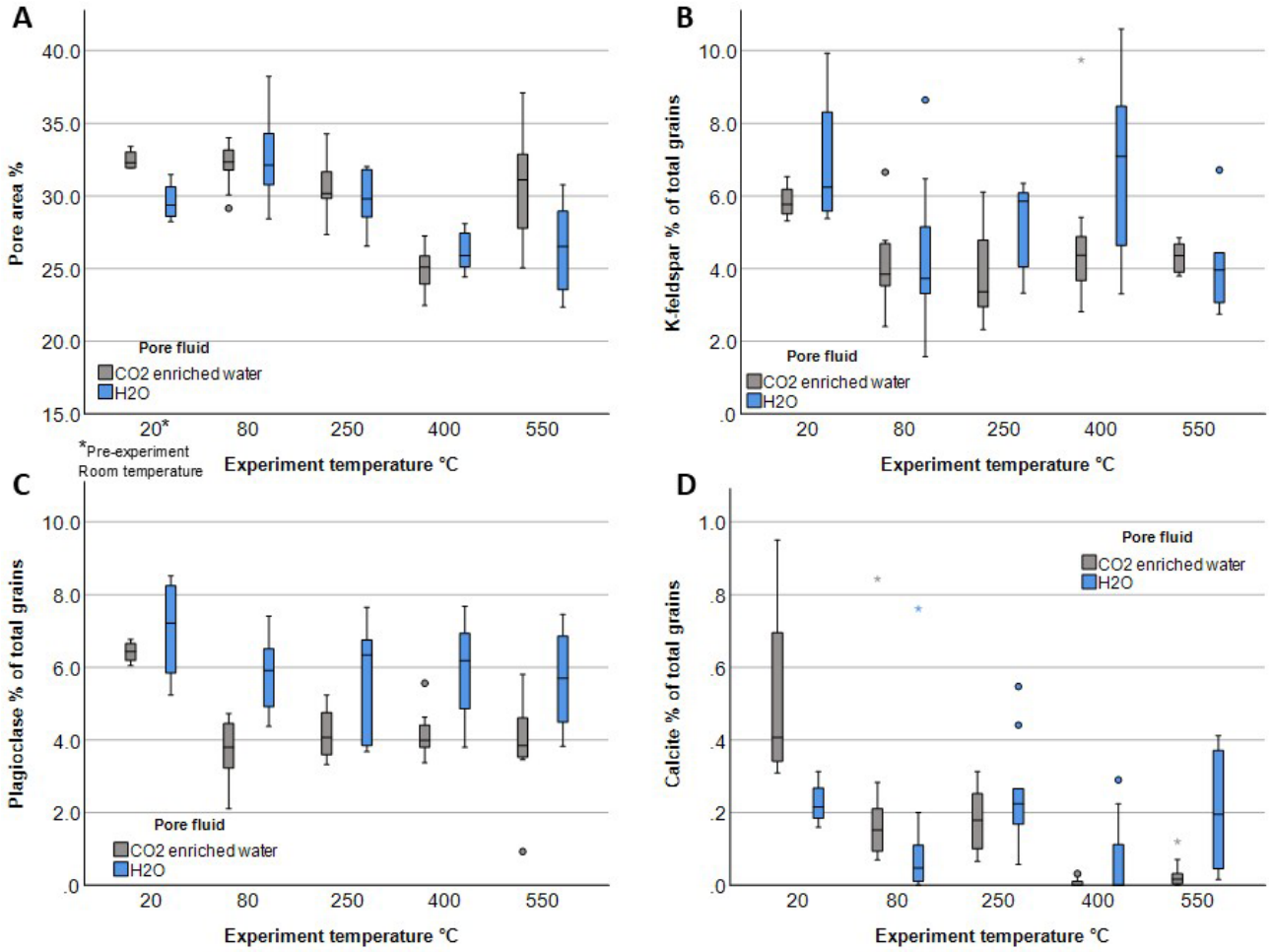

Figure 11. Box and whisker plots d in pore area and reactive mineral content in Captain Sandstone samples before and after reaction, experiments, based on thresholded EDS images. Two pre-reaction samples, "Dt" and "Dm", with slightly different bulk compositions were used: Dm cores (H_2O experiments) and Dt cores (CO_2 experiments), shown in grey and blue, respectively. Box plots display data spread, including median, interquartile range (IQR), and outliers.

clude: (1) early incongruent dissolution of K-feldspar in CO_2 experiments conducted at 80 °C, as CO_2-enriched fluids, weakened grains and promoted microfracturing; (2) extensive congruent dissolution K-feldspar in higher temperature > 250 °C experiments with CO_2, which resulted in grain size reduction, creation of secondary pores and increase in pore area; (3) near-complete dissolution of calcite grains and cements in CO_2 experiments, compared to partial dissolution with H_2O; and (4) partial dissolution and incongruent leaching of calcium from oligoclase grains from 80 °C with CO_2, resulting in grain area reduction that was not observed in H_2O experiments, (Fig. 11). Reactions, deformation mechanisms observed in experiments are summarised in Table 2 and key mineral phases present in the Cretaceous Captain sandstone before, during and after experiments are highlighted in Fig. 12.

4.1.1 Feldspar deformation and reaction textures

Our results show that at reservoir temperatures CO_2 enriched fluids created a chemically reactive environment that promoted compositionally preferential, incongruent dissolution of K-feldspar and oligoclase. In K-feldspar this produced parallel porous "seams" that developed on the edge of grains, possibly exploiting cleavage planes (Fig. 5A). These features were absent in higher temperature experiments, possibly because (1) they represented early-stage dissolution textures that were overprinted by later grain dissolution or (2) experiments at higher temperatures (above 250 °C) produced a shift in the dominant reaction mechanism from ion exchange reactions (i.e. early incongruent release of K^+, Na^+, and Ca^{2+}) to hydrolysis-driven dissolution (i.e. congruent breakdown of the Si-O framework). Similar temperature-dependent dissolution styles have been observed in previous feldspar reaction

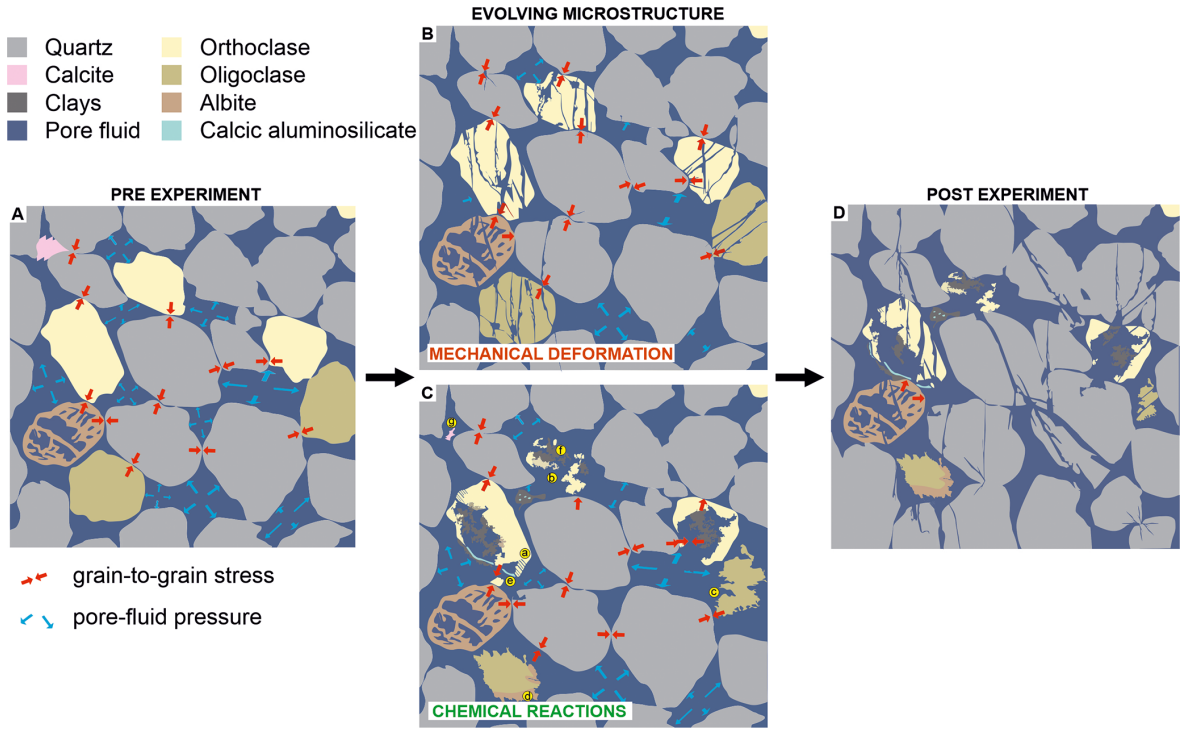

Figure 12. Schematic summary of the coupled mechanical and chemical changes identified from hydrostatic batch experiments using CO_2-enriched pore fluids on the Captain Sandstone ("D sand"). Experiments were conducted at reservoir-relevant confining and pore fluid pressures, generating grain to grain scale stresses at temperatures of 80–550 °C. These conditions promote interacting mechanical and chemical feedbacks that drive the evolution of sandstone microstructure and texture. **(A)** Pre-experimental sandstone texture with intact K-feldspar (orthoclase), calcic plagioclase (oligoclase), skeletal albite, and minor calcite cement. **(B)** Mechanical deformation preferentially fractures feldspars relative to quartz, creating fresh reactive surfaces and increasing feldspar–fluid contact. **(C)** Chemical reactions include (a) orthoclase dissolution expressed as parallel cracks penetrating from grain margins to interiors, (b) orthoclase grain dissolution, (c) oligoclase dissolution, (d) albitisation of oligoclase, (e) precipitation of calcic aluminosilicate, (f) precipitation of clay minerals (muscovite–illite), and (g) dissolution of calcite cement. **(D)** Post-experiment analysis illustrates how coupled deformation–dissolution and new mineral precipitation reshape the microstructure.

experiments on microcline (Fung et al., 1980), albite (Chen et al., 2000), and labradorite (Carroll and Knauss, 2005).

K-feldspars with incongruent dissolution textures produced at lower reservoir temperatures appeared to be mechanically weaker and more susceptible to the effects of grain-to-grain stresses under confining pressure, which led to microfracturing and crushing between the more resistant quartz grains (Figs. 4, S5–S7). In turn, these "fresh" microfractures and fragmented grains created more reactive surfaces, which drove further dissolution in a positive feedback loop of "incongruent dissolution, stress-induced microfracture, and enhanced grain reactivity". This process likely accelerated the significant K-feldspar comminution and dissolution textures observed after higher temperature experiments.

In plagioclase, interaction with CO_2-enriched fluid had no apparent effect on albite grains but oligoclase showed partial dissolution, evident as wavy grain boundaries and localised compositional zoning (Fig. 8). EDS analysis indicated that this texture was formed by incongruent dissolution, with calcium being selectively leached from the edge of grains leaving a sodium rich outer zone around an intact Ca-Na rich grain centre (Fig. 8). A thin Ca-rich rim at the grain edge was also observed. While grain weakening evidenced by microfracturing was less evident in altered oligoclase grains, pressure solution features (e.g., concave–convex contacts) suggests stress-driven mass transfer played a role in the evolution of these dissolution textures.

4.1.2 Coupled dissolution-precipitation and ion exchange

At > 400 °C in both H_2O and CO_2 experiments, K-feldspar dissolution was coupled with secondary mineral precipitation. This included pore-filling masses, overgrowths and fracture fills of calcic aluminosilicate rims and K-bearing clays associated with dissolving K-feldspar grains (Figs. 5D and S14). Despite the sharp boundary between the primary K-feldspar and secondary calcic aluminosilicates, optical continuity between secondary phases and host grains indi-

cates epitaxial growth via ion exchange as Ca^{2+} in the pore fluid was substituted for K^+ in K-feldspar. Quantitative surface area analysis showed K-feldspar and calcite as dominant dissolving phases in H_2O and CO_2 experiments (Fig. 1). While incongruent dissolution of oligoclase in CO_2 experiments contributed additional Ca^{2+} via leaching (Fig. 8). The resulting enrichment likely induced supersaturation, triggering precipitation of calcic aluminosilicates and potassic aluminosilicates (K-clays) (Fig. 5).

Similar coupled dissolution-precipitation (CDP) reactions in K-feldspar have previously been observed both in nature (Cole et al., 2004, Moore et al., 2005; Baines and Worden; 2004) and experiments (Putnis et al., 2007b; Niedermeier et al., 2009; Norberg et al., 2011; Abart et al., 2012). For example, albitisation of sanidine and orthoclase by Na-Cl fluids via CDP produced sharp reaction interfaces with crystallographically aligned albite overgrowths (Norberg et al., 2011). In another experimental study, the replacement of albite by K-feldspar produced sharply defined reaction fronts while preserving the crystallographic orientation of the host grain (Niedermeier et al., 2009). Additionally, similar to the parallel dissolution seams observed in our study, Niedermeier reported aligned "tubular nanopores" normal to the replacement interface which they interpreted as pathways for fluid access to the reaction front (Niedermeier et al., 2009). Such nanotube formation appears to be a common feature of reaction fronts in mineral lattices (Harlov et al., 2005; Zeitler et al., (2017).

4.1.3 Anorthitisation of K-feldspar comparison to previous studies

In this study, we observed the replacement of K-feldspar by calcic aluminosilicates i.e. "anorthitisation", under experimental conditions (400 °C, 70 MPa confining pressure). Anorthitisation has been described in natural systems, e.g. the transformation of andesine to anorthite in the presence of Ca^{2+}-rich meteoric fluids (Mora et al., 2009) and has been described conceptually in the framework of CDP reactions (Putnis, 2009). Though K-feldspar alteration via direct K^+-Ca^{2+} substitution has not been described previously in geological settings, there are natural examples of K-feldspar alteration involving Ca-bearing fluids. These include high temperature hydrothermal systems where K-feldspar is replaced by Na-Ca plagioclase and myrmekite textures form via K, Na, and Ca exchange (Chakrabarty et al., 2023). And low temperature settings in CO_2-rich basins like Otway and Bravo Dome where fluid acidification drives feldspar dissolution and precipitation of Ca-bearing phases such as dawsonite and calcic zeolites, (Mora et al., 2009; Wigley et al., 2013; Baines and Worden, 2004).

While the replacement of K-feldspar by calcic aluminosilicates via ion exchange has not been previously described under controlled laboratory conditions in geoscience, it has been explored and established in materials science. Specifically, anorthitisation via ion exchange is being investigated as a method for extracting potassium from K-feldspar using calcium-bearing fluids as an alternative method for fertiliser production. Although not yet commercially implemented, laboratory studies have shown K^+ leaching from K-feldspar powders at temperatures as low as 65 °C (Ma et al., 2016; Ciceri et al., 2017), and the formation of calcic aluminosilicate phases, texturally similar to those observed in our experiments, at 160 °C (Liu et al., 2015; Haseli et al., 2020; Zhai et al., 2021). These findings suggest that ion exchange via CDP observed in our study may represent a previously unrecognised mechanism for K-feldspar alteration in the presence of CO_2-enriched fluids.

4.1.4 Source of calcium

In natural systems, Ca^{2+} is typically derived from hydrothermal fluids or CO_2-enirched waters that leach calcium from carbonates, plagioclase, or mafic phases. In our experiments, elevated calcium in the pore fluid resulted from (1) dissolution of calcite grains and cement, prominent in all CO_2 experiments, and to a lesser degree in H_2O experiments > 400 °C, and (2) partial dissolution of oligoclase, observed only in CO_2 experiments. Incongruent dissolution of plagioclase is well established, for example, a previous experimental study on labradorite showed that calcium release rates exceeded silica release by a factor of three, highlighting strongly incongruent behaviour (Knauss and Wolery, 1986). This likely explains why we observed preferential calcium leaching from oligoclase, producing a Na-rich rim around an intact Na-Ca grain core. The precipitation of secondary calcic aluminosilicate phases may have further contributed to calcium leaching, as the removal of Ca^{2+} from the pore fluid enhanced chemical disequilibrium and promoted continued oligoclase dissolution.

Previous studies on the Captain Sandstone "D sand" also observed calcite dissolution during CO_2 flow-through experiments at < 60 °C (Hangx et al., 2015). However, this study focused on the effect of calcite dissolution on rock mechanical strength and, although they also noted K-feldspar dissolution, did not examine the coupled mechanisms driving geochemical alteration or potential for ion exchange.

4.1.5 Role of stress

Although our experiments were successfully designed to limit mechanical compaction (confirmed by maintenance of pore area in H_2O and CO_2 runs up to 250 °C), features indicative of chemical compaction via pressure solution, such as concave–convex grain contacts, were observed in both H_2O and CO_2 experiments above 400 °C. These suggest localised, stress-assisted dissolution at grain contacts under high temperature aka faster reaction rate experiments. This dissolution likely increased local K^+ concentration, providing micro-zones of supersaturation and promoting precip-

itation in adjacent lower-stress areas around grain boundaries. Analogous features are seen in natural CO_2 reservoirs like the Supai Sandstone Formation, where dawsonite precipitates are spatially associated with corroded K-feldspar and in the Triassic Chaunoy Formation, which associates feldspar dissolution textures with carbonate and zeolite formation (Moore et al., 2005; Baines and Worden, 2004, respectively).

4.2 Comparison to previous studies on CO_2 : sandstone interaction

The enhanced dissolution of K-feldspar and calcite in CO_2-enriched fluids observed in our study aligns with previous experimental studies. For instance, a 3 month CO_2 flow-through experiment at 140 °C resulted in K-feldspar dissolution, grain size reduction, and secondary porosity, leading to a 20 % increase in porosity and increased permeability (Hall et al., 2015). Although no secondary precipitation occurred due to constant undersaturation, deformation textures e.g. altered feldspars and secondary porosity, closely resemble observations from our experiments. In addition to the dissolution of calcite cement noted in the Hangx study described above, carbonate mineral dissolution in sandstones reacted with CO_2-enriched fluids is experimentally well established. Several studies have shown increased calcium concentrations in pore fluids following saturation of sandstone samples with CO_2-enriched brines, many accompanied by a corresponding permeability increase (Ross et al., 1982; Sayegh et al., 1990; Hall et al., 2020; Foroutan et al., 2021). Precipitation of secondary phases was apparently not a limiting factor for K-feldspar dissolution in our experiments, contrasting with the experimental results of Lu et al., (2013), possibly due to fracture-induced increases in feldspar-fluid surface area.

Studies on feldspar alteration in geological CO_2-injection projects and natural CO_2 reservoirs also support our findings. In a study on the microstructural impact of CO_2 on sandstone in an engineered subsurface setting, the microstructure of pre- and post-core CO_2 flood sandstones from the Pembina Cardium CO_2 Monitoring Project in Canada showed partial dissolution of K-feldspar grains after 2 years of CO_2 injection (Nightingale et al., 2020). And as previously noted, natural CO_2 reservoirs such as Bravo Dome also show feldspar alteration and secondary mineral formation linked to long-term CO_2 exposure (Wigley et al., 2013). These findings confirm that feldspar alteration and associated secondary porosity development can occur over relatively short timescales in the subsurface and are comparable in character to the features we have observed in our higher-temperature experimental system.

4.3 Implications for CCS reservoirs

Our findings have several *direct* implications for geological storage of CO_2. Firstly, they demonstrate that K-feldspar and oligoclase in CO_2-enriched fluids at reservoir-relevant conditions can undergo rapid alteration including grain microcracking, dissolution and the development of secondary porosity. Second, they show that dissolution of even small amounts (e.g. 1 %) of calcite grains and cement or leaching of calcium from plagioclase can elevate Ca^{2+} concentrations in the pore fluid and, depending on local fluid composition and saturation states, promote ion exchange with K-feldspar and drive the precipitation of calcic aluminosilicates and K-bearing clays. Third, the presence of pressure solution textures suggests that local stress concentrations create grain-scale chemical disequilibria, enhancing feldspar dissolution and promoting localised mineral precipitation, processes that are often overlooked in geochemical models of CCS systems.

These microstructural alterations have important implications for reservoir integrity and CCS project performance. Fracturing and dissolution of framework feldspars ($\sim$ 16 % of the D sand) could reduce compressive strength, alter elastic properties, and modify porosity. These properties are key parameters in both geomechanical and fluid flow models and could alter the predicted reservoir behaviour. Such changes would be especially critical near structural features like faults, where shifts in strength or porosity may alter fault stability during fluid injection/depletion. While the relatively unfaulted Acorn CCS site may be less susceptible to fault reactivation, microstructural changes such as feldspar fracturing and dissolution could still lead to mechanical compaction and reservoir fracturing. The impact of this may affect the ability to flow CO_2 fluids into the reservoir, i.e. productivity. However, in some cases, such as the Ekofisk field, reservoir collapse and compaction have paradoxically enhanced permeability and improved production (Teufel et al., 1991).

Secondary mineral precipitation, such as K-bearing illite, could reduce permeability and hinder CO_2 injection/migration, but feldspar dissolution, especially of Ca-bearing phases like oligoclase may enhance long-term CO_2 sequestration by releasing Ca^{2+}. that can become incorporated into secondary phases, possibly even locking in carbon. However, if Ca^{2+} instead bonds with dissolving K-feldspar, it may reduce carbonate formation and limit carbon trapping through mineralisation. Dawsonite did not form in our experiments, likely due to the low Na and Cl content of our fluids. In natural CCS settings, brine compositions with higher Na concentrations could promote dawsonite or other Na-bearing phase formation via K-feldspar replacement. Instead, we observed formation of a calcic aluminosilicate, although we cannot confirm whether it contained carbon, as our carbon-coated thin sections compromised EDS detection.

4.4 Experimental limitations

While our findings offer empirical evidence for feldspar reactivity in CO_2-enriched fluids, several limitations are acknowledged. Most notably, the elevated temperatures used in some experiments accelerated reaction kinetics beyond those

typical of natural systems. However, the occurrence of similar dissolution reactions, albeit to a lesser extent, at reservoir temperatures supports the relevance of our results to CCS reservoir and a comparison to reaction rates on a geological timescale has been calculated (Supplement). Post-quench precipitation of secondary phases cannot be ruled out, although the presence of well-crystallised calcic aluminosilicate in optical continuity with host grains strongly suggest that these minerals formed in situ during the experiments. This interpretation is consistent with previous work which noted similar limitations and applied the same criteria to distinguish in-experiment from post experiment precipitation (Rosenqvist et al., 2019).

For this study, we employed batch reactor experiments because they allow direct comparison with the geochemical models used in the Acorn CCS Project (Shell, 2015. Batch systems are optimal for studying both dissolution and precipitation processes as they more closely mimic the generally static fluid conditions in subsurface reservoirs than flow through setups. However, batch reactors do not simulate the effects of fluid flow, which in a CCS reservoir would significantly influence reaction kinetics as the dissolved phases would be transported, both reducing supersaturation and making for a dynamic ongoing pore fluid chemistry. As previous CO_2 : sandstone flow-through experiments have shown, undersaturation of the fluid suppresses precipitation but enhances feldspar dissolution (Hall et al., 2015). For understanding the interplay between reaction rate and transport in dynamic subsurface environments like CCS reservoirs, both experimental styles are important. Another limitation is the use of tap water rather than brine. Although selected to avoid the overly reactive behaviour of deionised water, our fluid lacks the high Na^+ and Cl^+ content typical of formation waters, which may influence both dissolution and secondary mineral precipitation. Future work should incorporate brine compositions and use flow-through systems under triaxial stress to better simulate reservoir conditions.

Despite these limitations, our results provide some of the first experimental evidence for CO_2 fluid induced K-feldspar alteration under controlled conditions relevant to CCS subsurface settings. This supports the idea that K^+–Ca^{2+} exchange can occur via coupled dissolution–precipitation mechanisms, with implications for feldspar reactivity, reservoir evolution, and long-term mineral trapping in CCS scenarios.

5 Summary

This study offers new insights into mineral transformations and grain-scale deformation in a planned CCS reservoir – processes that have been previously recognised in CO_2 : sandstone studies but never systematically investigated. This study also provides the first geological evidence that Ca^{2+} released from experimental dissolution of detrital feldspar grains in a sandstone (i.e. not freshly ground-up powder) can drive in-situ K^+ – Ca^{2+} ion exchange in K-feldspar under realistic subsurface conditions.

Consistent with our hypothesis, experimental results showed that:

1. K-feldspar is more reactive than expected when exposed to disequilibrium fluids (both H_2O and CO_2) under subsurface hydrostatic stresses at temperature; and

2. in comparison to H_2O, CO_2-enriched fluids significantly altered solubility of both plagioclase and K-feldspar and produced distinct microstructural changes even during short (6 d) experiments.

At reservoir temperatures (80 °C), CO_2-enriched fluids induced incongruent dissolution and deformation of K-feldspar and dissolution of detrital calcite via ion exchange underscoring the relevance of these transformations to CCS settings. At higher temperatures, where reaction kinetics were accelerated, both H_2O and CO_2 fluids promoted dissolution of reactive minerals – K-feldspar, oligoclase, and calcite – leading to the precipitation of secondary aluminosilicate and clay phases. We propose that these transformations reflect a coupled dissolution–precipitation mechanism, where Ca^{2+} released from calcite and oligoclase dissolution activates and sustains K-feldspar alteration and subsequent dissolution. Crucially, the formation of epitaxial Ca-bearing overgrowths on K-feldspar grains provides clear experimental evidence for K^+ – Ca^{2+} ion exchange. While this anorthitisation of K-feldspar has been engineered in materials science studies using Ca-rich fluids, this study is the first to demonstrate the reaction occurring in situ – i.e., within intact rock, under subsurface stress using weakly CO_2-enriched fluids.

As discussed, previous experimental and natural studies show that feldspar alteration can involve coupled dissolution, ion exchange, and secondary mineral formation. Our findings build on this by demonstrating more varied modes of feldspar transformation with CO_2-enriched and calcium bearing fluids. While consistent with earlier CO_2- sandstone work, this study uniquely combines microstructural and geochemical changes created under known conditions to map possible reaction pathways and quantify the impact on mineral texture and microstructure. These processes, often difficult to capture in reactive transport models, could significantly affect reservoir properties like pore volume, fluid flow, and geomechanical integrity.

Outlook on remaining challenges

Chemical mapping and compositional analyses suggest that feldspar zoning may influence dissolution behaviour, although further investigation is required. The original chemical homogeneity of the feldspars and their provenance appear to be important factors controlling reactivity, which could have implications for other arkosic reservoir systems. More

broadly, this study raises new questions about the timing and mechanisms of feldspar reactivity in stressed, fluid-saturated environments. It demonstrates the need to reconsider CCS appraisal approaches, which often assess geochemical and geomechanical behaviour separately. Our findings support a more integrated understanding of these processes and have wider relevance for other subsurface applications, including geothermal energy and mineral extraction. Finally, quantifying feldspar dissolution kinetics remains a key challenge due to the formation of secondary clays and interactions with other phases. Future work should focus on simplified, monomineralic synthetic systems with controlled textures and grain sizes to isolate, and thereby better constrain, reaction rates.

Data availability. All data supporting this study are publicly available in the Supplement and via Figshare. Supplementary figures (Figs. S6–S8), XCT images, and animations are archived in Figshare and accessible through https://doi.org/10.6084/m9.figshare.30061294.v1 (Farrell et al., 2025). No third-party data were used.

Supplement. The supplement related to this article is available online at https://doi.org/10.5194/se-17-407-2026-supplement.

Author contributions. Design of this project and acquisition of funding were carried out by NF, MF, and KT. NF designed the experiments and prepared samples, and PDRA's LY and NB carried them out. LP provided technical support i.e. tooling, fixing the rig pump. MF and LH collected SEM BSE and EDS images. NF, MF, CM and MP conducted analysis of microstructural and geochemical data. BA and KT collected XCT data and processed and analysed the images. JW carried out XRD analysis. NF prepared the manuscript with contributions from all co-authors.

Competing interests. The contact author has declared that none of the authors has any competing interests.

Disclaimer. Publisher's note: Copernicus Publications remains neutral with regard to jurisdictional claims made in the text, published maps, institutional affiliations, or any other geographical representation in this paper. The authors bear the ultimate responsibility for providing appropriate place names. Views expressed in the text are those of the authors and do not necessarily reflect the views of the publisher.

Acknowledgements. Funding was provided by the Engineering and Physical Sciences Research Council (EPSRC) through IDRIC Project FF 4-13. Additional support for knowledge exchange and collaboration between the research team and industry partners was provided by a UK Research and Innovation (UKRI) Impact Acceleration Award. N. J. C. Farrell acknowledges support from a Leverhulme Early Career Fellowship Award. M. J. Flowerdew acknowledges support from the industrial sponsors of the Cambridge Arctic Shelf Programme (CASP). We also thank Scott Renshaw and the team at the British Geological Survey National Geological Repository for assistance with sampling.

Financial support. This research has been supported by the UK Research and Innovation (grant no. IDRIC Project FF 4-13).

Review statement. This paper was edited by Petr Jeřábek and reviewed by Laura Airaghi and Alexis Cartwright-Taylor.

References

Abart, R., Petrishcheva, E., and Joachim, B.: Thermodynamic model for growth of reaction rims with lamellar microstructure, American Mineralogist, 97, 231–240, https://doi.org/10.2138/am.2011.3820, 2012.

Akhurst, M., Blanco Sánchez, P. H., Kirk, K., Mosca, I., Pierce, J., Williams, J., Flowerdew, M., Joss, M., Jahanbakhsh, A., Marr, I., Fraga, D., Trusler, M., Farrell, N., Nixon, S., Walker, L., Armstrong, L.-M., Dbouk, W., Manias, P., Teagle, D., Turnock, S., Vakili, S., Minto, J. M., and Roberts, J. J.: IDRIC Frontiers Report: Carbon Capture and Storage (CCS) – Spotlight: CO_2 Transport and Storage, https://doi.org/10.2139/ssrn.5505958, 2025.

Alcalde, J., Heinemann, N., Mabon, L., Worden, R. H., De Coninck, H., Robertson, H., Maver, M., Ghanbari, S., Swennenhuis, F., Mann, I., and Walker, T.: Acorn: Developing full-chain industrial carbon capture and storage in a resource- and infrastructure-rich hydrocarbon province, Journal of Cleaner Production, 233, 963–971, https://doi.org/10.1016/j.jclepro.2019.06.087, 2019.

Allen, M. J., Faulkner, D. R., Worden, R. H., Rice-Birchall, E., Katirtsidis, N., and Utley, J. E.: Geomechanical and petrographic assessment of a CO_2 storage site: Application to the Acorn CO2 Storage Site, offshore United Kingdom, International Journal of Greenhouse Gas Control, 94, https://doi.org/10.1016/j.ijggc.2019.102923, 2020.

Baines, S. J. and Worden, R. H.: The long-term fate of CO_2 in the subsurface: natural analogues for CO_2 storage, in: Geological Storage of Carbon Dioxide, edited by: Baines, S. J. and Worden, R. H., Geological Society Special Publication 233, Geological Society, London, UK, 59–85, https://doi.org/10.1144/GSL.SP.2004.233.01.06, 2004.

Benson, S. M. and Cole, D. R.: CO_2 sequestration in deep sedimentary formations, Elements, 4, 325–331, https://doi.org/10.2113/gselements.4.5.325, 2008.

Bertier, P., Swennen, R., Laenen, B., Lagrou, D., and Dreesen, R.: Experimental identification of CO_2–water–rock interactions caused by sequestration of CO_2 in Westphalian and Buntsandstein sandstones of the Campine Basin (NE-Belgium), Journal of Geochemical Exploration, 89, 10–14, https://doi.org/10.1016/j.gexplo.2005.11.005, 2006.

Blum, A. E. and Stillings, L. L.: Feldspar dissolution kinetics, in: Chemical Weathering Rates of Silicate Minerals, Reviews in Mineralogy, Vol. 31, edited by: Brantley, S. L., Ameri-

can Mineralogical Society, Washington, DC, USA, 291–351, https://doi.org/10.1515/9781501509650-009, 1995.

Brantley, S. L., Kubicki, J. D. and White, A. F. (Eds.): Kinetics of Water-Rock Interaction, Reviews in Mineralogy and Geochemistry, Vol. 168, Mineralogical Society of America and Geochemical Society, Chantilly, VA, USA, 281 pp., ISBN 9780939950819, 2008.

Carroll, S. A. and Knauss, K. G.: Dependence of labradorite dissolution kinetics on $CO_{2(aq)}$, $Al_{(aq)}$, and temperature, Chemical Geology, 217, 213–225, https://doi.org/10.1016/j.chemgeo.2004.12.008, 2005.

Chakrabarty, A., Mukherjee, S., Karmakar, S., Sanyal, S., and Sengupta, P.: Petrogenesis and in situ U-Pb zircon dates of a suite of granitoid in the northern part of the Central Indian tectonic Zone: Implications for prolonged arc magmatism during the formation of the Columbia supercontinent, Precambrian Research, 387, 106990, https://doi.org/10.1016/j.precamres.2023.106990, 2023.

Chen, Y., Brantley, S. L., and Ilton, E. S.: X-ray photoelectron spectroscopic measurement of the temperature dependence of leaching of cations from the albite surface, Chemical Geology, 163, 115–128, https://doi.org/10.1016/S0009-2541(99)00096-0, 2000.

Ciceri, D., de Oliveira, M., and Allanore, A.: Potassium fertilizer via hydrothermal alteration of K-feldspar ore, Green Chemistry, 19, 5187–5202, https://doi.org/10.1039/C7GC02633A, 2017.

Cole, D. R., Larson, P. B., Riciputi, L. R., and Mora, C. I.: Oxygen isotope zoning profiles in hydrothermally altered feldspars: Estimating the duration of water-rock interaction, Geology, 32, 29–32, https://doi.org/10.1130/G19881.1, 2004.

Collettini, C., Tesei, T., Scuderi, M. M., Carpenter, B. M., and Viti, C.: Beyond Byerlee friction, weak faults and implications for slip behavior, Earth and Planetary Science Letters, 519, 245–263, https://doi.org/10.1016/j.epsl.2019.05.011, 2019.

Correns, C. W.: Experiments on the decomposition of silicates and discussion of chemical weathering, in: Clays and Clay Minerals (National Conference on Clays and Clay Minerals) (Vol. 10, 443–459), Cambridge University Press & Assessment, https://doi.org/10.1346/CCMN.1961.0100139, 1961.

Dove, P. M. and Crerar, D. A.: Kinetics of quartz dissolution in electrolyte solutions using a hydrothermal mixed flow reactor, Geochimica et cosmochimica acta, 54, 955–969, https://doi.org/10.1016/0016-7037(90)90431-J, 1990.

Durst, P. and Vuataz, F. D.: Fluid-rock interactions in hot dry rock reservoirs: a review of the HDR sites and detailed investigations of the Soultz-sous-Forêts system, in: Proceedings of the World Geothermal Congress 2000, Kyushu–Tohoku, Japan, June 2000, 3677–3682, 2000.

Farrell, N. J. C. and Healy, D.: Anisotropic pore fabrics in faulted porous sandstones, Journal of Structural Geology, 104, 125–141, https://doi.org/10.1016/j.jsg.2017.09.010, 2017.

Farrell, N. J. C., Debenham, N., Wilson, L., Wilson, M. J., Healy, D., King, R. C., Holford, S. P., and Taylor, C. W.: The effect of authigenic clays on fault zone permeability, Journal of Geophysical Research: Solid Earth, 126, https://doi.org/10.1029/2021JB022615, 2021.

Farrell, N. J. C., Yang, L., Flowerdew, M. J., Mark, C., Ardo, B., Taylor, K. G., Bigaroni, N., Pointon, M., Hughes, L., Waters, J., and Paul, L.: XCT images and animations, Figshare, Version 1, https://doi.org/10.6084/m9.figshare.30061294.v1, 2025.

Flowerdew, M. J., Farrell, N., Yang, L., Badenszki, E., Mark, C., Ardo, B., and Taylor, K.: Feldspars in CCS reservoirs: overlooked or unimportant?, in: CCS4G Symposium 2024, London, UK, CCS4G-Symposium-2024-Abstracts.pdf, 2024.

Folk, R. L., Andrews, P. B., and Lewis, D. W.: Detrital sedimentary rock classification and nomenclature for use in New Zealand, New Zealand Journal of Geology and Geophysics, 13, 937–968, https://doi.org/10.1080/00288306.1970.10418211, 1970.

Foroutan, M., Ghazanfari, E., and Amirlatifi, A.: Variation of failure properties, creep response and ultrasonic velocities of sandstone upon injecting CO_2-enriched brine, Geomechanics and Geophysics for Geo-Energy and Geo-Resources, 7, https://doi.org/10.1007/s40948-021-00223-y, 2021.

Fuchs, S. J., Espinoza, D. N., Lopano, C. L., Akono, A. T., and Werth, C. J.: Geochemical and geomechanical alteration of siliciclastic reservoir rock by supercritical CO_2-saturated brine formed during geological carbon sequestration, International Journal of Greenhouse Gas Control, 88, 251–260, https://doi.org/10.1016/j.ijggc.2019.06.014, 2019.

Fung, P. C., Bird, G. W., McIntyre, N. S., Sanipelli, G. G., and Lopata, V. J.: Aspects of feldspar dissolution, Nuclear Technology, 51, 188–196, https://doi.org/10.13182/NT80-A32600, 1980.

Glasmann, J. R.: The fate of feldspar in Brent Group reservoirs, North Sea: A regional synthesis of diagenesis in shallow, intermediate, and deep burial environments, Geological Society, London, Special Publications, 61, 329–350, https://doi.org/10.1144/GSL.SP.1992.061.01.17, 1992.

Hall, M. R., Rigby, S. P., Dim, P., Bateman, K., Mackintosh, S. J., and Rochelle, C. A.: Post-CO2 injection alteration of the pore network and intrinsic permeability tensor for a Permo-Triassic sandstone, Geofluids, 16, 249–263, https://doi.org/10.1111/gfl.12146, 2015.

Hangx, S. J. and Spiers, C. J.: Coastal spreading of olivine to control atmospheric CO_2 concentrations: A critical analysis of viability, International Journal of Greenhouse Gas Control, 3, 757–767, https://doi.org/10.1016/j.ijggc.2009.07.001, 2009.

Hangx, S., Bakker, E., Bertier, P., Nover, G., and Busch, A.: Chemical–mechanical coupling observed for depleted oil reservoirs subjected to long-term CO_2-exposure–A case study of the Werkendam natural CO_2 analogue field, Earth and Planetary Science Letters, 428, 230–242, https://doi.org/10.1016/j.epsl.2015.07.044, 2015.

Harlov, D. E., Wirth, R., and Förster, H. J.: An experimental study of dissolution–reprecipitation in fluorapatite: fluid infiltration and the formation of monazite, Contributions to Mineralogy and Petrology, 150, 268–286, https://doi.org/10.1007/s00410-005-0017-8, 2005.

Haseli, P., Majewski, P., Christo, F., Raven, M., Klose, S., and Bruno, F.: Experimental kinetic analysis of potassium extraction from ultrapotassic syenite using NaCl–$CaCl_2$ salt mixture, Acs Omega, 5, 16421–16429, https://doi.org/10.1021/acsomega.0c00549, 2020.

Helgeson, H. C., Murphy, W. M., and Aagaard, P.: Thermodzhuynamic and kinetic constraints on reaction rates among minerals and aqueous solutions. II. Rate constants, effective surface area, and the hydrolysis of feldspar, Geochimica et Cosmochimica Acta, 48, 2405–2432, https://doi.org/10.1016/0016-7037(84)90294-1, 1984.

Hellmann, R., Wirth, R., Daval, D., Barnes, J. P., Penisson, J. M., Tisserand, D., Epicier, T., Florin, B., and Hervig, R. L.: Unifying natural and laboratory chemical weathering with interfacial dissolution–reprecipitation: a study based on the nanometer-scale chemistry of fluid–silicate interfaces, Chemical Geology, 294, 203–216, https://doi.org/10.1016/j.chemgeo.2011.12.002, 2012.

IPCC: Special Report on Carbon Dioxide Capture and Storage, Cambridge University Press, Cambridge, 431, ISBM 978-0-521-86643-9, 2005.

Juanes, R., Spiteri, E. J., Orr Jr, F. M., and Blunt, M. J.: Impact of relative permeability hysteresis on geological CO_2 storage, Water Resources Research, 42, https://doi.org/10.1029/2005WR004806, 2006.

Knauss, K. G. and Wolery, T. J.: Dependence of albite dissolution kinetics on pH and time at 25 °c and 70 °c, Geochimica et Cosmochimica Acta, 50, 2481–2497, https://doi.org/10.1016/0016-7037(86)90031-1, 1986.

Liu, S. K., Han, C., Liu, J. M., and Li, H.: Hydrothermal decomposition of potassium feldspar under alkaline conditions, Rsc Advances, 5, 93301–93309, https://doi.org/10.1039/C5RA17212H, 2015.

Lu, P., Fu, Q., Seyfried Jr, W. E., Hedges, S. W., Soong, Y., Jones, K., and Zhu, C.: Coupled alkali feldspar dissolution and secondary mineral precipitation in batch systems–2: New experiments with supercritical CO_2 and implications for carbon sequestration, Appl. Geochem., 30, 75–90, https://doi.org/10.1016/j.apgeochem.2012.04.005, 2013.

Ma, X., Ma, H., and Yang, J.: Sintering preparation and release properties of $K_2MgSi_3O_8$ slow-release fertilizer using biotite acid-leaching residues as silicon source, Industrial & Engineering Chemistry Research, 55, 10926–10931, https://doi.org/10.1021/acs.iecr.6b02991, 2016.

Moore, J., Adams, M., Allis, R., Lutz, S., and Rauzi, S.: Mineralogical and geochemical consequences of the long-term presence of CO_2 in natural reservoirs: an example from the Springerville–St. Johns Field, Arizona, and New Mexico, USA, Chemical Geology, 217, 365–385, https://doi.org/10.1016/j.chemgeo.2004.12.019, 2005.

Mora, C. I., Riciputi, L. R., Cole, D. R., and Walker, K. D.: High-temperature hydrothermal alteration of the Boehls Butte anorthosite: origin of a bimodal plagioclase assemblage, Contributions to Mineralogy and Petrology, 157, 781–795, https://doi.org/10.1007/s00410-008-0364-3, 2009.

Niedermeier, D. R., Putnis, A., Geisler, T., Golla-Schindler, U., and Putnis, C. V.: The mechanism of cation and oxygen isotope exchange in alkali feldspars under hydrothermal conditions, Contributions to Mineralogy and Petrology, 157, 65–76, https://doi.org/10.1007/s00410-008-0320-2, 2009.

Nightingale, M., Johnson, G., Shevalier, M., Hutcheon, I., Perkins, E., and Mayer, B.: Impact of injected CO_2 on reservoir mine ralogy during CO2-EOR, Energy Procedia, 1, 3399–3406, https://doi.org/10.1016/j.egypro.2009.02.129, 2020.

Norberg, N., Neusser, G., Wirth, R., and Harlov, D.: Microstructural evolution during experimental albitization of *K*-rich alkali feldspar, Contributions to Mineralogy and Petrology, 162, 531–546, https://doi.org/10.1007/s00410-011-0610-y, 2011.

Pessu, F., Macente, A., Sanni, O., and Piazolo, S.: The importance of whole system considerations for sustainable, long-term CO_2 injection and storage: Interplay between infrastructure-related corrosion and reservoir rock chemistry effects on the evolution of the CO_2 storage capacity, International Journal of Greenhouse Gas Control, 148, 104520, https://doi.org/10.1016/j.ijggc.2025.104520, 2025.

Pinnock, S. J., Clitheroe, A. R. J., and Rose, P. T. S.: The Captain Field, Block 13/22a, UK North Sea, TS39, Geological Society of London Memoirs, 20, https://doi.org/10.1144/GSL.MEM.2003.020.01.35, 2003.

Putnis, A.: Mineral replacement reactions, Reviews in Mineralogy and Geochemistry, 70, 87–124, https://doi.org/10.2138/rmg.2009.70.3, 2009.

Putnis, C. V., Geisler, T., Schmid-Beurmann, P., Stephan, T., and Giampaolo, C.: An experimental study of the replacement of leucite by analcime, American Mineralogist, 92, 19–26, https://doi.org/10.2138/am.2007.2249, 2007.

Rathnaweera, T. D., Ranjith, P. G., Perera, M. S. A., Haque, A., Lashin, A., Al Arifi, N., Chandrasekharam, D., Yang, S. Q., Xu, T., Wang, S. H., and Yasar, E.: CO_2-induced mechanical behaviour of Hawkesbury sandstone in the Gosford basin: An experimental study, Materials Science and Engineering: A, 641, 123–137, https://doi.org/10.1016/j.msea.2015.05.029, 2015.

Ringrose, P.: How to store CO_2 underground: Insights from early-mover CCS projects, SpringerBriefs in Earth Sciences, Springer International Publishing, Cham, Switzerland, 129, https://doi.org/10.1007/978-3-030-33113-9, 2020.

Rochelle, C. A., Czernichowski-Lauriol, I., and Milodowski, A. E.: The impact of chemical reactions on CO_2 storage in geological formations: a brief review, Geological Society of London Memoirs, 233, https://doi.org/10.1144/GSL.SP.2004.233.01.07, 2004.

Rosenqvist, J., Kilpatrick, A. D., Yardley, B. W., and Rochelle, C. A.: Alkali feldspar dissolution in response to injection of carbon dioxide, Applied Geochemistry, 109, 104419104419, https://doi.org/10.1016/j.apgeochem, 2019.

Ross, G. D., Todd, A. C., Tweedie, J. A., and Will, A. G.: The dissolution effects of CO_2-brine systems on the permeability of UK and North Sea calcareous sandstones, in: SPE Improved Oil Recovery Conference (SPE-10685), SPE, https://doi.org/10.2118/10685-MS, 1982.

Rutter, E. H.: A discussion on natural strain and geological structure-the kinetics of rock deformation by pressure solution, Philosophical Transactions of the Royal Society of London. Series A, Mathematical and Physical Sciences, 283, 203–219, https://doi.org/10.1098/rsta.1976.0079, 1976.

Sayegh, S. G., Krause, F. F., Girard, M., and DeBree, C.: Rock-/fluid interactions of carbonated brines in a sandstone reservoir: Pembina Cardium, Alberta, Canada, SPE formation evaluation, 5, 399–405, https://doi.org/10.2118/19392-PA, 1990.

Scholz, C. H.: Static fatigue of quartz, Journal of Geophysical Research, 77, 2104–2114, https://doi.org/10.1029/JB077i011p02104, 1972.

Seisenbayev, N., Absalyamova, M., Alibekov, A., and Lee, W.: Reactive transport modeling and sensitivity analysis of CO_2–rock–brine interactions at Ebeity Reservoir, West Kazakhstan, Sustainability, 15, 14434, https://doi.org/10.3390/su151914434, 2023.

Shell: Peterhead CCS Project: Geochemical Reactivity Report, Doc. No. PCCS-05-PT-ZR-3323-00001, produced by Shell U. K. Limited for the UK CCS Commercialisation Programme, Goldeneye CO_2 storage project, 2015.

Shogenov, K., Shogenova, A., Vizika-Kavvadias, O., and Nauroy, J. F.: Experimental modeling of CO_2-fluid-rock interaction: The evolution of the composition and properties of host rocks in the Baltic Region, Earth and Space Science, 2, 262–284, https://doi.org/10.1002/2015EA000105, 2015.

Stewart, N. and Marshall, J. D.: The Goldeneye Field, Blocks 14/29a and 20/4b, UK North Sea, Geological Society of London Memoirs, 52, https://doi.org/10.1144/M52-2018-32, 2020.

Summers, R. and Byerlee, J.: A note on the effect of fault gouge composition on the stability of frictional sliding, in: International Journal of Rock Mechanics and Mining Sciences & Geomechanics Abstracts (Vol. 14, No. 3, 155–160), Pergamon, https://doi.org/10.1016/0148-9062(77)90007-9, 1977.

Teufel, L. W., Rhett, D. W., and Farrell, H. E.: 1991, July. Effect of reservoir depletion and pore pressure drawdown on in situ stress and deformation in the Ekofisk field, North Sea, in: ARMA US Rock Mechanics/Geomechanics Symposium, ARMA-91-063, 1991.

Tullis, J. and Yund, R. A.: A Experimental deformation of dry Westerly granite, Journal of Geophysical Research, 82, 5705–5718, https://doi.org/10.1029/JB082i036p05705, 1977.

Wigley, M., Dubacq, B., Kampman, N., and Bickle, M.: Controls of sluggish, CO_2-promoted, hematite and K-feldspar dissolution kinetics in sandstones, Earth and Planetary Science Letters, 362, 76–87, https://doi.org/10.1016/j.epsl.2012.11.045, 2013.

Whitney, D. L. and Evans, B. W.: Abbreviations for names of rock-forming minerals, American Mineralogist, 95, 185–187, https://doi.org/10.2138/am.2010.3371, 2010.

Wollast, R.: Kinetics of the alteration of K-feldspar in buffered solutions at low temperature, Geochimica et Cosmochimica Acta, 31, 635–648, https://doi.org/10.1016/0016-7037(67)90040-3, 1967.

Wheeler, J.: A view of texture dynamics, Terra Nova, 3, 123–136, https://doi.org/10.1111/j.1365-3121.1991.tb00864.x, 1991.

Zeitler, P. K., Enkelmann, E., Thomas, J. B., Watson, E. B., Ancuta, L. D., and Idleman, B. D.: Solubility and trapping of helium in apatite, Geochimica et Cosmochimica Acta, 209, 1–8, https://doi.org/10.1016/j.gca.2017.03.041, 2017.

Zhai, Y., Hellmann, R., Campos, A., Findling, N., Mayanna, S., Wirth, R., Schreiber, A. Cabié, M., Zeng, Q., Liu, S., and Liu, J.: Fertilizer derived from alkaline hydrothermal alteration of K-feldspar: micrometer to nanometer-scale investigation. Applied Geochemistry, 126, https://doi.org/10.1016/j.apgeochem.2020.104828, 2021.